

**APPLICATION OF DIFFUSION
TECHNIQUES TO THE SEGMENTATION OF
MR 3D IMAGES FOR VIRTUAL
COLONOSCOPY**

LE MANOUR FREDERIC

NATIONAL UNIVERSITY OF SINGAPORE

2007

APPLICATION OF DIFFUSION TECHNIQUES TO
THE SEGMENTATION OF MR 3D IMAGES FOR
VIRTUAL COLONOSCOPY

LE MANOUR FREDERIC

(B.Eng. (Hons), Supélec)

A THESIS SUBMITTED
FOR THE DEGREE OF MASTER OF ENGINEERING
DEPARTMENT OF ELECTRICAL & COMPUTER ENGINEERING
NATIONAL UNIVERSITY OF SINGAPORE

2007

Abstract

Due to technological advances, computer tomography virtual colonoscopy systems have been a very active research topic and can now be found commonly in clinical use. MR imaging techniques could offer greater possibilities for virtual colonic examinations due to their unrivaled imaging of soft tissues and non radiating nature; however, this has not been possible until today because of the data acquisition limitations. In this study we will investigate the possibility of using magnetic resonance images for virtual colonic systems. To cope with the low signal to noise ratio of images, diffusion techniques in both the isotropic and anisotropic schemes are considered, which allows reducing the noise in the images while enhancing the frontier formed by the inner colon wall. The general ideas and theoretical foundations behind anisotropic diffusion and its relation to scale space transformations are analyzed, as well as their discrete aspects and concrete implementation in 3D. The results of diffusion are then used to derive a new adaptive thresholding segmentation technique. This technique is applied to segment the inner colon wall boundary, which opens the way to virtual colonoscopy based on MR imaging.

Acknowledgment

I would like to express my sincere appreciation and gratitude to my supervisors, Assoc. Prof. Ong Sim Heng, as well as Dr. Yan Chye Hwang, for their advice, guidance and assistance throughout the course of this project.

I would also like to thank Mr. Francis Hoon from the Vision and Image Processing laboratory for his assistance during the entire course of this research.

I am especially grateful to Yeo Eng Thiam.

Last but not least, I would like to extend my appreciation to all those who have helped me one way or another during this project.

Frederic Le Manour

November 11, 2007

Contents

1	Introduction	1
1.1	Motivation	1
1.2	Aim of the Thesis	3
1.3	Contributions of the Thesis	5
1.4	Organization of the Thesis	5
2	Literature Review	7
2.1	Use of MR in Virtual Colonoscopy	7
2.2	Anisotropic Diffusion of MR Images	9
2.3	Segmentation Techniques of MR Images	10
3	Acquisition and Characteristics of Images	13
3.1	Medical Considerations	13
3.2	Scanning Protocol	14
3.3	Characteristics of the Images	15
4	Presentation of Diffusion Techniques	19
4.1	Physical Background of Diffusion and Terminology	19
4.2	Scale Space in the Linear Framework	21
4.2.1	Definition	21
4.2.2	Gaussian example	23
4.3	Anisotropic Diffusion	23
4.3.1	The Perona and Malik model	24

4.3.2	Energy minimisation	26
4.3.3	Tensor diffusion	28
4.4	Directional Analysis of Anisotropic Diffusion	29
4.5	Summary	32
5	Implementation of Diffusion Techniques for Noise Reduction	34
5.1	Choice of Functions	34
5.2	Regularization	38
5.3	Numerical and Discrete Schemes	40
5.4	Choice of Parameters	44
5.5	Results and Comparison	47
5.5.1	Analysis of parameters and diffusion techniques	47
5.5.2	Application to MR abdominal images	53
5.5.3	Comparison with other noise removal techniques	57
5.6	Conclusion	59
6	Segmentation of the Colon for Virtual Colonoscopy	60
6.1	Objectives	60
6.2	Global Segmentation Algorithm	61
6.3	Automatic Seed Selection	64
6.4	Local Threshold Computation	65
6.5	Results	66
6.6	Discussion	69
6.6.1	Consequences of diffusion on the segmentation results	69
6.6.2	Reliability of the segmentation process	70
6.7	Use of Segmentation Results in Virtual Colonoscopy	71
6.7.1	Conventional use	71
6.7.2	Future Work	73
7	Conclusion	76

A Intermediate Results of the Segmentation Algorithm	79
---	-----------

B Segmentation Results	82
-------------------------------	-----------

List of Figures

2.1	Conventional (left) and virtual (right) colonoscopy images of the same pedunculated polyp in the sigmoid colon	8
3.1	Anatomy of the large intestine	14
3.2	Typical slice of dataset, coronal view	16
4.1	Gaussian scale space	23
4.2	Non-linear scale space	25
5.1	Diffusivity functions	37
5.2	Test image	47
5.3	Analysis of the diffusion scheme	49
5.4	Influence of the contrast parameter	51
5.5	Influence of the diffusivity function	52
5.6	Diffusion scale spaces	54
5.7	Diffusion scale spaces, zoom of Fig. 5.6	55
5.8	Comparison of noise reduction techniques	58
6.1	Global segmentation algorithm overview	62
6.2	Local features used for adaptive thresholding	67
6.3	Segmented colon	68
6.4	Endoscopic view of a polyp	68
6.5	Endoscopic view of the segmented colon	72
6.6	Virtual colonoscopy software	73

A.1	Seed points resulting from automatic seed selection	79
A.2	Rough segmented colon after global segmentation and region growing	80
A.3	Incomplete threshold map after computation of thresholds at the edge points	80
A.4	Complete threshold map after interpolation	81
A.5	Final segmented result after adaptive thresholding and region growing	81
B.1	Segmented result of slice 19 of dataset MRC712	82
B.2	Segmented result of slice 27 of dataset MRC712	83
B.3	Segmented result of slice 41 of dataset MRC712	83
B.4	Segmented result of slice 60 of dataset MRC712	84

List of Tables

1.1	Screening methods	2
5.1	Diffusivity functions	35
5.2	Discretization models	41

Chapter 1

Introduction

1.1 Motivation

Cancers of the rectum and colon are together the third most common type of cancer and the second most common cause of cancer death in the US [1] with more than 55000 deaths and 140000 newly diagnosed cases each year [2]. While precursor lesions such as adenomas¹ and colon polyps² are commonly silent, they almost always precede the development of cancer by several years. Screening the colon at an early stage to detect these lesions could help identify the disease at a point when cure or control is still potentially possible and could prevent cancers from occurring.

Since most symptoms develop at an advanced stage of the illness, it is desirable to act in a preventive manner to detect the lesions when they are still benign. Screening techniques have been developed for viewing the inside of the colon. A summary of the numerous possibilities can be found in Table 1.1.

Virtual Colonoscopy (VC) is a new technique that allows doctors to look at the large bowel (colon) to detect polyps in a non invasive approach. Volumetric datasets are acquired by either computed tomography (CT) and magnetic reso-

¹Adenomas: benign growths of glandular origin that are known to have the potential, over time, to transform to malignancy. If it becomes cancerous, it is called an adenocarcinoma

²Polyps are fleshy growths on the inside (the lining) of the colon and rectum

Table 1.1: Screening methods

Technique	Barium En-ema	Colonoscopy	CT	MRI
Dimension	2D	Video: 2D+t	3D	3D
Radiation	Yes ($\approx 10\text{mSv}$)	No	Yes (≈ 5 to 10 mSv)	No
Resolution	Moderate	Very good	Good	Low
Sensitivity ³	Low	Good	Good	Not tested
Cost	Low	High (physician needed for long time)	Moderate	High
Use	Screening, low cost, low effectiveness, now nearly abandoned for other techniques	Screening and treatment, gold standard but long and uncomfortable	Screening, fast expanding, more patient friendly	Screening, no commercial system available yet

nance (MR) systems, post processed and used in virtual reality software so that the radiologist can perform a virtual exploration to examine the interior of the colon. The rendered endoluminal views of the colon interior simulate the view of a endoscope camera navigating the reconstructed model of the colon. Automatic fly-through as well as manual navigation are proposed to help the radiologist in arriving at a diagnosis. The aim of such a system is to build a virtual environment that provides the same protocols as for a virtual endoscopy. The non-invasive nature of VC that results in less procedural pain and discomfort is undoubtedly already a significant improvement over conventional colonoscopy, but VC has the possibility for much more. The visualization techniques are not limited to the simulation of the endoscopic view, and the next step for VC is to add features to VC that would bring true added value compared to conventional colonoscopy, such as automatic polyp detection and new visualization techniques that would speed up the radiologist's task.

Technological advances over the past 20 years have enabled many medical imaging systems to be designed and implemented and among those MRI (magnetic resonance imaging) has seen tremendous improvement in the last few years. Revo-

³Sensitivity: percentage of affected patients recognized by the clinical test

lutionizing many medical practices, MRI has become one of the most used imaging systems; however, the capacities of MRI are still far from being fully employed. VC has been a very active area of research for the past 15 years and commercial systems are now widely available, but they still rely on CT images and no MR VC system can be found today in commercial use. Nonetheless, an increasing number of clinicians are turning to MR for their examinations. In the context where abdominal screening should become a routine examination to undergo every few year (5 to 10 years) [3], the doses of ionizing radiation induced by CT colonography⁴ have been considerably reduced [4] but are still a concern even when the benefit to risk ratio is considered as large [5]. MR imaging would get rid of this concern due to its non-ionizing radiation nature. Moreover, MRI is preferred to CT for the imaging of soft tissue since it offers better contrast between tissues and the possibility to use contrast agents to further enhance some of few features that have to be analyzed. MR imaging has also some inherent drawbacks most importantly slow acquisition times compared to CT. The quality of the acquired data is directly linked to the length of the acquisition time and patient need to hold their breath during the full time of the acquisition. However, the need for MR-based systems is important, as some radiologists already prefer working with MR scans but have to go through 2D visualization of slices and mentally align them. Although this gives reasonably good results [6, 7, 8], it still has to be further enhanced to emerge as a consistent screening method. An automated process would not only save time and reduce costs for both patients and doctors, but it could also lower the risk of missing polyps, thus providing a higher diagnostic accuracy.

1.2 Aim of the Thesis

In the present work we consider the feasibility of a virtual colonoscopy (VC) system based on MR images. The goal is, therefore, to obtain a 3D model of the colon

⁴The term colonography is synonymous with virtual colonoscopy. *-graphy* is a suffix coming from the Greek for *to write* which indicates here the need for an imaging technique rather than an endoscope.

from an MR abdominal scan covering the patient's entire colon, and to use that model to detect polyps. Once the colon is segmented from the acquired images, this can be achieved using the same visualization techniques as for CT virtual colonoscopy, namely either automatic fly-through or manual navigation. According to medical stipulations, the objective is to obtain perfect sensitivity for polyps of larger than 10mm and high sensitivity for polyps between 5 to 10mm. To meet such requirements, the segmentation of the colon's structure will need to be performed with high accuracy even for the smallest structures.

Humans are expert in recognizing patterns and structures, and the ease with which this is achieved does not give any hint on the real complexity of the processes in the human brain. Even in the cases when there is severe noise, we are highly efficient in recognizing structures; however, many image processing techniques require high signal to noise ratios (SNRs) because most segmentation techniques are very sensitive to noise. Medical images are often characterized by high SNR and low contrast, or inversely, high contrast and low SNR. The human eye can perform strongly in both cases while computer-based techniques have difficulties working on images with low SNR. If MRI has still so many unexplored possibilities, it is mainly because the processing techniques are not adapted to the MR images with low SNRs and relatively high contrast, which suit the human eye better.

To take into consideration the high requirements of the segmentation and the low quality of the datasets, we will investigate the use of noise reduction techniques before the proper segmentation algorithm for more accurate results. Among the numerous noise reduction methods that can exist, recent developments have shown the strength of diffusion techniques, and more specifically, anisotropic diffusion for medical images. We choose to work on anisotropic diffusion techniques to take advantage of their noise reduction potential associated with the unrivaled contour localization they offer. An in-depth analysis of such techniques will show that their use is highly effective in the present case, and how their implementations can be done efficiently. Comparison with other techniques will show that this choice

is justified. An automatic segmentation scheme will then be derived from the diffusion results, which further consolidates the results of the diffusion process and enables us to consider MR virtual colonoscopy in its full scope.

1.3 Contributions of the Thesis

The contributions of the thesis are summarized here.

- An important work of unification has been done on diffusion techniques to come out with a coherent framework that builds a path toward tensor based techniques.
- The inconsistency of the image processing community on the terminology *anisotropic diffusion* has been explained and some ideas are proposed to the reader to let him make his own judgment.
- The implementation of anisotropic diffusion with the fast AOS scheme has been done in 3D.
- It has been shown that we can make use of anisotropic diffusion techniques in a precise framework for accurate enhancement of the inner boundary of the colon wall.
- A new segmentation algorithm based on the properties of edge enhancing diffusion has been derived. We make use of the diffusion results to develop an adaptive thresholding scheme which has been applied to perform the segmentation of the colon wall in the datasets.
- The alternative of using MR acquisition techniques instead for computer tomography for virtual colonoscopy has been investigated.

1.4 Organization of the Thesis

The outline of the thesis is as follows:

Chapter 2 After the survey of the current status of MRI in its use for virtual colonoscopy, a literature review of the main topics used in this thesis is presented, namely the usage of anisotropic diffusion techniques for MR images and the segmentation methods of medical MR images.

Chapter 3 The environment of the project is presented, from the medical considerations of virtual colonoscopy to the scanning protocol used to obtain the datasets and their characteristics.

Chapter 4 The theoretical aspects of diffusion are described in a way to guide the reader naturally from the physical background of diffusion to the more complicated anisotropic schemes that are useful in the current work.

Chapter 5 This chapter will deal with the concrete implementation of the process used as a pre-segmentation denoising step. The discretization problems as well as the choice of parameters are studied to build a consistent algorithm. The results are presented and compared with other techniques.

Chapter 6 We deal with the segmentation of the data resulting from the pre-segmentation step. An fully automatic process is presented and the results are analyzed.

Chapter 7 Concluding remarks, overall analysis, and futures perspectives are presented.

Chapter 2

Literature Review

2.1 Use of MR in Virtual Colonoscopy

MR imaging has had a very late development in its use for virtual colonoscopy. The first conventional colonoscopies were performed in the 1960s in Japan due to the development of the colonoscope and while CT based systems are now available commercially, MR based screenings studies are still lacking, and are the subject of numerous feasibility studies.

The first study which was really aimed at building a true virtual colonoscopy system based on MR images was done by a research group from the State University of New York, Stony Brook, in the years 1998-1999 [9]. The lack of ionizing radiation was their major appeal for working with MR protocols, at the time when everyone was investigating CT techniques for VC.

The theoretical possibility to differentiate, in MR images, between soft tissues, and more specifically between the colon wall and the other soft tissues was from the beginning the ultimate goal for all MR VC segmentation processes. When looking at a 3D rendered views on a conventional CT VC system, the radiologists have to base their diagnosis only on the shapes of the structures that are visible. CT imaging does not offer any possibility of visualization of soft tissues; hence only the inner colon wall boundary is segmented from the images. Although this

is close to how conventional colonoscopy is performed, during the latter procedure the radiologist can also rely on the texture of the interior colon wall and on the colors is visualises (Fig. 2.1).

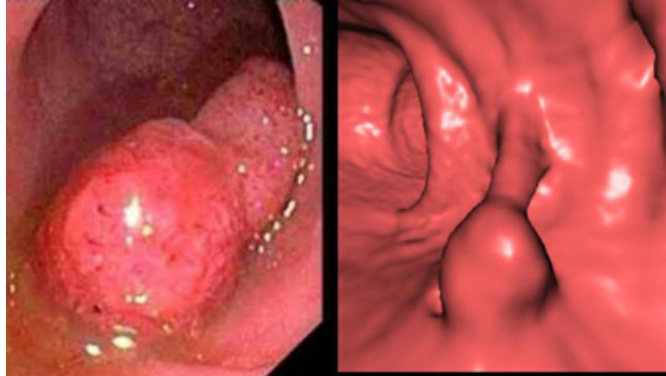


Figure 2.1: Conventional (left) and virtual (right) colonoscopy images of the same pedunculated polyp in the sigmoid colon²

If the entire colon wall in its full thickness can be distinguished on the MR images, then the radiologist is able to use other features for his examination: the colon wall thickness that gives information on the possibility of a tumor (especially in the case of flat polyps) as well as the change in intensity. Adding those features in a VC software could definitely facilitate the doctor's task.

These advanced possibilities with MR VC were spotted from the first study and can be found in subsequent ones. However, a major task stayed in the way of the achievement of a usable system: the segmentation of those features and most importantly of the inner boundary of the colon wall. While for the CT images this can be segmented out with relative ease, it is much more difficult with MR images. In the Stony Brook preliminary study the dataset used was formed by T2-weighted coronal images with 6mm inter-slice, for a total acquisition time of 1 minute [9]. While the unrealistic acquisition time is not of much importance for a feasibility study, the 6mm inter-slice to detect polyps of 10mm or less shows that a clinical usage is still dependent on major technological improvements, despite promising results.

²adapted from <http://www.med.nyu.edu/virtualcolonoscopy/images/VC1.jpg>

To cope with this, many studies were then centered on MR acquisition techniques, in order to find a fast scanning protocol offering good contrast between the colon wall, the surrounding soft tissues (attached to the outer surface of the colon) and the inside. With the need of acquiring a dataset providing good anatomical detail in one breath hold, fast T1-weighted imaging gradient echo sequences have rapidly become a standard in many MR imaging protocols. To cope with the serious constraints imposed by virtual colonoscopy, a volumetric interpolated breath-hold examination (VIBE) sequence was proposed by Rofsky et al [10]. This will be described later in Section 3.2 since this protocol will be used for my experimentations.

A logical question also comes from the filling of the colon for data acquisition. Once the colon is cleansed, it has to be distended for better visualization and both air or water can be used. The discomfort by both techniques are of similar levels [11] and it has been shown that the contrast to noise ratio (CNR) using air is better [11]. On top of this, contrast agents can be administered to provide better contrast between the inside and the colonic wall. While bright lumen was employed first, dark lumen has recently be found to be more advantageous [12] with the administration of gadolinium for enhancement of soft tissues.

2.2 Anisotropic Diffusion of MR Images

The goal of this section is to present the possible usage of anisotropic diffusion techniques with MR images. A complete literature review of anisotropic diffusion techniques could be a study on its own, therefore Chapter 4 will present the logical path which leads to the chosen implementation of the diffusion process.

The image processing methodology based on non-linear diffusion equations problems has been used to investigate enhancement and restoration of images. For both medical [13] as well as for geometrical problems [14], it has shown its strength in eliminating noise and artifacts while preserving large global features, such as object contours.

In the medical context it has shown to be very useful as a preprocessing step for MR imaging based techniques [15, 16, 17]. While MRI opens many possibilities, with superior contrast between soft tissues, many image processing techniques are highly dependent on the quality of the segmentation process. Segmentation has therefore become an increasingly important step for areas such as diagnosis, treatment, virtual surgery, image registration and in many cases it is the key step that will define the strength of a technique. Due to reasons that will be detailed in the following section, automatic segmentation is however a non-trivial problem. Anisotropic diffusion techniques have been used in some cases for the implementation of fully automatic segmentation algorithms, while in other cases only to increase their performance. Some studies have also tried to incorporate the diffusion process directly in the segmentation step instead of dissociating the two. Gradient vector flow (GVF) is, for example, a snake with external forces based on a diffusion process [18] while anti-geometric diffusion tries to build a adaptive thresholding segmentation algorithm using the properties of the diffusion process [19].

2.3 Segmentation Techniques of MR Images

The characteristics of MR images make segmentation a very challenging task. Low SNR, partial volume effect, and a wide range of parameters are major obstacles toward the automation of segmentation, which is needed in a medical context where a fast, accurate and reproducible segmentation is a prerequisite for evaluation, diagnosis and treatment. Fully automated segmentation are obviously the ultimate goal of all segmentation algorithms. However the trade-off between fully automatic and semi automatic methods has to be taken into consideration when prior knowledge of an operator can improve significantly the accuracy of the results. This is often the case when minimum user interaction while defining the initialization parameters can act positively upon the rest of the algorithm.

A common difficulty for the segmentation of MR images comes from the non-

inhomogeneity inherent in the datasets, mainly when using surface coils, which can lower considerably the performance of usual segmentation techniques. Medical images are often also subject to the partial volume effect (PVE); the low sampling which is very frequent in MRI produces a structural definition ambiguity in which the boundaries of the different tissues or structures are hard to locate. A common technique to solve such problem is to allow soft segmentation, which contrary to hard segmentation does not enforce a binary decision whether the pixel is inside or outside the segmented region.

Thresholding and region growing techniques are the first and simplest methods that were developed and are now seldom used alone but often as a part of a complex segmentation process. The core algorithms of both techniques suffer from major drawbacks: sensitivity to noise and inhomogeneity, need for a seed point for region growing, tendency of results to be disconnected and have holes in the segmented regions. Many variations have been proposed to overcome those weaknesses, resulting in very efficient techniques in some specific cases.

Many segmentation algorithm developed recently were based on unsupervised clustering techniques such as *k-means*, *fuzzy-c-means* [20, 21] or *expectation-maximization* [22]. Those methods expand the possibilities of thresholding techniques by trying to find automatically some optimality for each class. However they do not incorporate spatial information and suffer from the same disadvantages as previously. To increase the robustness of such methods, Markov random fields models were introduced to model the interaction between neighboring pixels. While computationally intensive, it can be hard to select the parameters that control the spatial interaction; however, some studies have shown promising results, brain MR segmentation [23] being one example. An interesting example for virtual colonoscopy can be found in [24] although it is based on CT images.

Recently, deformable models have been popular in segmentation of medical images [25, 26]. A deformable model is a contour or surface, which deforms in order to capture objects to be segmented. The deformation is guided by forces, which can

be determined by features in the image (edges, texture) to be segmented, but also by geometric constraints (smoothness of the curve or surface; prior information of the shape to be segmented). The trade-off between geometric and image-derived information lies at the basis of the popularity and diversity of deformable model based methods; if image information alone is insufficient for a proper segmentation, the combination with geometric constraints may still yield plausible solutions. The techniques bears some drawbacks such as initialization and convergence toward concave boundaries which can be problematic issues [27]. Deformable models can be found under many different types of parametrization and representations, and very good reviews can be found covering the subject [28, 29]

Once a segmentation method is developed its performance has to be quantified in order to assess its accuracy. This is a challenging task in medical imaging where sometimes radiologists can have difficulties in performing manual segmentation. A common practice is to validate the model against manually obtained segmentations, although the result cannot be considered of perfect truth since the manual segmentation can also be flawed.

Chapter 3

Acquisition and Characteristics of Images

3.1 Medical Considerations

The large intestine is the portion of the digestive system most responsible for absorption of water from the indigestible residue of food. It begins at the ileocecal junction where material passes from the ileum to the cecum (large intestine) and ends with the rectum and the anal canal, being in total about 1.5m long. It is comprised of 4 main parts (Fig. 3.1): the ascending colon roughly starts after the appendix and cecum and continues up to the right (hepatic) flexure. After the right flexure, the colon continues with the transverse colon. It travels across the abdomen to the left (splenic) flexure. The descending colon begins after the left flexure and leads to the sigmoid colon, and ultimately to the rectum. The ascending and descending colons are fixed to the pelvic wall. In contrast, the transverse colon has more freedom to move; it is only suspended on a peritoneal fold.

The objective of virtual colonoscopy is to detect cancerous polyps which are abnormal growth of tissue (tumor) projecting a the mucous membrane. Colon polyps are a concern because of the potential for colon cancer being present mi-

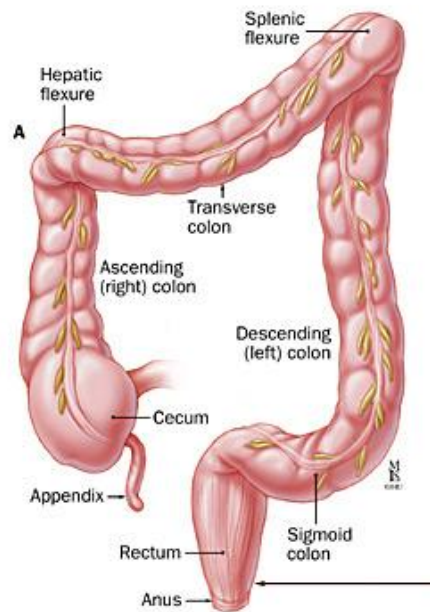


Figure 3.1: Anatomy of the large intestine¹

croscopically and the risk of benign colon polyps transforming with time into colon cancer. It has been shown [30] that polyps of less than 10mm have a very low probability of being malignant; however this probability increases rapidly with the size of the tumor. It is in consequence of highest importance that all structures of 10mm or more can be well visualized and must not be deteriorated by any processing. Achieving the same results for polyps between 5 to 10mm would also be appreciated in the objective of cancer surveillance.

3.2 Scanning Protocol

MR colonography techniques require proper patient preparation prior to scanning. For good visualization two requirements are of major importance: sufficient distension of the colonic lumen and sufficient contrast between the colonic wall and the lumen. To fulfill the first requirement a bowel relaxant is administered to the patient prior to scanning. It helps in obtaining a improved distension as well as re-

¹adapted from http://hopkins-gi.nts.jhu.edu/pages/latin/templates/index.cfm?pg=disease5&organ=6&disease=32&lang_id=1

ducing motion artifact of the colon during the acquisition of the dataset. To ensure proper distension the colon is also filled with air. MR scanning protocol is chosen such as to obtain a good contrast as mentioned above, and intravenous administration of a gadolinium solution is performed prior acquisition to enhance contrast of soft tissues. It improves the SNR since the colonic wall becomes brighter leading to images of significantly better quality for processing, but has the drawback to increase cost significantly.

The sequence used for MR colonography is a 3D T1-weighted FLASH volumetric interpolated breath-hold examination with fat selective pre-pulse sequence, commonly known as VIBE sequence. First described by Rofsky *et al* [10], the VIBE sequence is a 3D gradient recalled echo sequence which is commonly used in contrast enhanced examinations of the abdomen. To reduce acquisition time of the 3D scan, a partial Fourier acquisition is performed in the z direction of k -space. The need for a short acquisition time technique arises from the need to get the acquisition of the full abdomen to be done in one breath hold so as to get maximum visualization space and minimum movements. Techniques providing high resolution datasets can last up to a few minutes, while a breath hold should not have to last longer than 20 seconds for clinical practice which sets very demanding constraints.

The current protocol combines both prone and supine scans to resolve ambiguities such as for stool rests, as well a pre and post contrast agent administration scans which gives information on tissue absorption of gadolinium.

3.3 Characteristics of the Images

The images produced by the acquisition process come in DICOM format with a header in which all scanning parameters are stored. The information is stored under 12 bits. The dataset is composed of around 80 to 90 images in coronal view (Fig. 3.2), with a section thickness of 2mm with no gap between slices, with that direction corresponding to the z direction of the k -space. It is important

to recall that since the dataset is acquired by a volumetric process, the dataset reconstructed by stacking all the images together can be considered as true voxels. The in-plane resolution of the images is of size 512×512 pixels, with a field of view of 500mm.



Figure 3.2: Typical slice of dataset, coronal view

The spatial resolution is a major inconvenience in MR imaging due to long acquisition times. The polyp detection objective being not to miss any polyp of 10mm or more and to obtain high sensitivity (the percentage of affected patients recognized by the clinical test) for polyps between 5 to 10 mm, it would seem adequate to have an isotropic resolution of 1mm. Under current technological advances, it is not possible to obtain a full abdominal scan with the last mentioned resolution, hence we will use re-sampling in order to obtain isotropic voxels. This will not improve the quality of the details in the z direction since it does not add any information to the data, it will only resample the dataset to isotropic voxels which is easier to use for processing. We have to keep in mind however for analysis that the details are acquired with a resolution higher than 1mm in the z . For the following processing algorithms, the dataset is resampled to 1mm isotropic voxels using a bi-cubic interpolation. Bicubic interpolation is a high order interpolation based on a cubic function which ensures the smoothness of the

function, the derivative and cross derivatives which preserves satisfactorily fine details [31].

Another possibility would lie in using multiple scans to have a complete coverage of the large intestine. This would enable us to have much better resolution, most importantly reducing the interslice distance to get true isotropic voxels. However it will not be considered here because the use of more than one scan would involve registration and fusion steps which would add important complexity to the problem.

MR imaging is known to be subject to many artifacts and the tight constraints of abdominal screening makes the data acquisition particularly prone to them. In the 3D gradient sequence of the protocol described above (3.2), the acquisition of the k -space occurs during the entire imaging time. As a result, the 3D MR sequence is very susceptible to motion artifacts. This is enforced by the nature of the scan: the patient has to hold his breath during a time which is close to the physical limits of many people. Moreover, a unavoidable cardiac artifact is known to occur due to the beats of the heart.

Another artifact which is typical of MR images is the intensity inhomogeneity artifact which produces a shading effect to appear over some part of the image. Although improvements in scanner technology have reduced this artifact significantly, inhomogeneities remain a problem particularly in images acquired by using surface coils. The size of the abdominal datasets make it highly likely that this artifact will corrupt at least some area in the images.

The requirements of high spatial resolution over a large area and high speed acquisition for abdominal screening lead to images with a relatively poor quality. The noise is clearly visible and some edges are hard to locate. Traditional methods to enhance image quality are acquisition based methods, either decreasing spatial resolution to increase voxel size to obtain a stronger signal, or lengthening acquisition time to obtain better noise reduction. As seen previously, acquisition methods are already pushed to their limit for VC, hence we will have to look at

post processing methods to restore noisy images efficiently and be able to get the needed features for VC.

Chapter 4

Presentation of Diffusion Techniques

4.1 Physical Background of Diffusion and Terminology

Diffusion, being the spontaneous spreading of matter (particles), heat, or momentum, is one type of transport phenomenon. It is the movement of particles from a higher potential to a lower one. This physical observation can be formulated in mathematical terms using the diffusion equation, which name changes accordingly with physics involved.

The equilibrium property of concentration is commonly known in steady state diffusion as *Fick's First Law*:

$$j = -D.\nabla u \tag{4.1}$$

This equation states that a flux j tries to compensate the concentration gradient ∇u according to the local diffusion tensor D .

The transport property without creation or destruction of mass can be ex-

pressed by the *continuity equation*:

$$\partial_t u = -\operatorname{div}(j) \quad (4.2)$$

with t representing time. Combining 4.1 into 4.2 yields the *diffusion equation*:

$$\partial_t u = \operatorname{div}(D \cdot \nabla u) \quad (4.3)$$

In image processing, the concentration u can be assimilated to the gray level of an image. In the present case we will be dealing with 3D images, hence: $u = u(x, t) : \mathbf{R}^3 \times [0; \infty[\rightarrow \mathbf{R}$ with $u(x, 0)$ being the initial image. The Diffusion tensor D can be a positive definite symmetric matrix or a scalar.

The computer vision literature is not unified on the terminology which derives from this equation. If D is function of the local structure of the image, Eq. (4.3) becomes a non-linear filter. From the work of Weickert [32], diffusion can only be anisotropic if D is not a identity matrix; in the scalar case, the diffusion is, from his framework, inhomogeneous and isotropic.

This terminology is inconsistent with Perona and Malik's fundamental work on anisotropic diffusion [33] and it has been shown later [34] that the Perona and Malik scalar's diffusion can be considered as anisotropic. Further analysis will be derived in the following sections to give the opportunity to the reader to make his own judgment. In this work, the classical terminology will be adopted instead of Weickert's.

- A diffusion will be called homogeneous when D is constant over the entire image, otherwise it will be called inhomogeneous.
- A diffusion will be considered non-linear when the function D is a non-linear function of the local structure of the image, otherwise it will be called linear.
- Both scalar and tensor diffusion will be called anisotropic

4.2 Scale Space in the Linear Framework

4.2.1 Definition

The objectives of noise filtering and approximation techniques are very similar in that they both tend toward simplifying an original image by making it smoother and with less local extrema. From this simplification ensues the scale notion; an image is formed of information at different levels of detail, for objects of different sizes and shown at different scales. The scale space transformation is the representation of the gradually simplified images derived from the original one. This representation makes possible the analysis at different scales to extract information that might not be as striking in the original image.

This idea is a vast area of research in its own and many papers have been published showing its depth and complexity such as [35, 36, 37, 38, 39]. Any work on image processing cannot ignore the strength of analysis it provides, and a brief taxonomy will be presented to highlight the positioning of our work.

- Discrete scale representation: This type of representation is useful for reducing stored information at higher scales. Various forms exist such as Burt's famous *pyramidal representation* [40] which has yielded important steps toward the scale space theory or Finkel and Bentley's *Quad-trees* [41].
- Linear continuous scale space: Many early works have contributed to the complete development of scale space theory as it is known today. Among those, Witkin [35, 42] has introduced Gaussian scale space filtering with Koenderink [36] deriving early scale space requirements; although the starting point of scale space research could be traced back to 1962 with the work of Iijima [43]. More than 10 set of axioms can be found in the literature, converging to the fact that Gaussian scale space is unique within a linear framework. A detailed analysis has been derived by Weickert [44], with Lindeberg coming out with a very approachable review on scale space theory [45].

- Non-linear continuous scale space: It comprises all image processing techniques that can be written as a non linear partial differential equation. Among those we can distinguish anisotropic diffusion which will be developed in following sections, linear morphological processes as developed by Alvarez, Guichard, Lions and Morel [46] and level set methods [47].

We define the scale space transformation as follows: let $u : \mathbf{R}^3 \rightarrow \mathbf{R}$ be the original image, from which the corresponding scale space can be formed by the group of gradually simplified version of it:

$$\{T_t u, \forall t \geq 0\}$$

provided it complies with the following requirements:

- Structural properties:
 - Localization property, which expresses that for a small t , $T_t u$ at the point x must be determined by the behaviour of u around x .
 - Continuity of T_t
 - Semigroup property, which states that:

$$\begin{aligned} T_0 u &= u, \quad \text{for } t = 0 \\ T_{t+s} u &= T_t(T_s u), \quad \forall t, s \geq 0 \end{aligned} \tag{4.4}$$

- Extremum principle (also known as minimum-maximum principle):

$$\inf_{\mathbf{R}^3} u \leq T_t u \leq \sup_{\mathbf{R}^3} u \tag{4.5}$$

It states that T_t must only reduce the image information; the transformation must not create new details that did not exist in the original image.

- Invariance property: two regions of u that can be linked by a rigid transformation must have the same scale space representation [48]

4.2.2 Gaussian example

If we come back to the general diffusion equation (Eq. (4.3)) and consider the simplest case where D is scalar and constant, we obtain the simple equation:

$$\partial_t u = \Delta u \quad (4.6)$$

This equation can be solved analytically and its solutions are well known: $u(x, t) = G_{\sqrt{2t}} \star u_0$ where G_σ is a Gaussian of standard deviation σ , and \star denotes convolution. This produces a Gaussian smoothing of the image which reduces noise but smoothens out edges and details in the image, as well as making more difficult the localization of details, which goes against the general idea of medical diagnosis. An example of a Gaussian scale space is presented in Fig. 4.1 where the curves correspond to increasing levels of simplification.

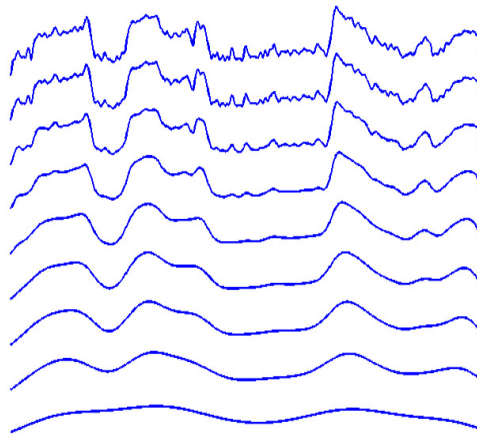


Figure 4.1: Gaussian scale space

4.3 Anisotropic Diffusion

As seen in the last example, we can appreciate that with a constant diffusivity over the all image, the diffusion process does not preserves edges. The precise localization of those edges cannot be done anymore at the larger scales since they

are blurred and dislocated by the diffusion. Due to the uniqueness of the Gaussian scale space in the linear framework, either the homogeneity, the linearity or some scale space assumptions will have to be dropped to overcome the problem.

4.3.1 The Perona and Malik model

Perona and Malik suggested the steering of the diffusion based on the local structure of the image by introducing a diffusivity function g dependent of both time (the scale parameter) and space [33]. The diffusion is controlled so that contours remain sharp and the smoothing occurs inside regions and not between regions. However to achieve these results, contours have first to be detected since they are not directly available in the image. This is done by using the local intensity gradient in the process as described by Perona and Malik. The new diffusivity equation can be written as:

$$\partial_t u = \operatorname{div}(g(|\nabla u|) \cdot \nabla u) \quad (4.7)$$

where g is the diffusivity function. Since the objective is to stop diffusion when contours are detected (high gradients) and let it flow inside homogeneous regions (low gradients) we would like to have the following properties for g :

$$g(0) = 1$$

$$\lim_{x \rightarrow \infty} g(x) = 0$$

Two function are proposed by Perona and Malik to fulfill those requirements:

$$g(x) = e^{-\left(\frac{x}{\lambda}\right)^2} \quad (4.8)$$

$$g(x) = \frac{1}{1 + \left(\frac{x}{\lambda}\right)^2} \quad (4.9)$$

λ plays the role of scale factor on the gradient: for gradient values higher than λ , the diffusion will be restrained, while for values lower than λ the diffusion will be important, and gradient values less than λ will hence be treated as noise.

This variation is quite smooth however; the pixels with gradient values close to λ have a very similar diffusion, and only after more iterations can the difference be appreciated.

Fig. 4.2 shows an example of nonlinear scale-space using the second diffusivity function (4.9) of Perona and Malik. The initial curve (top) is the same as the one used in the Gaussian example (Fig. 4.1), and curves represent increasing levels of simplification. The results with the Perona and Malik diffusion process are

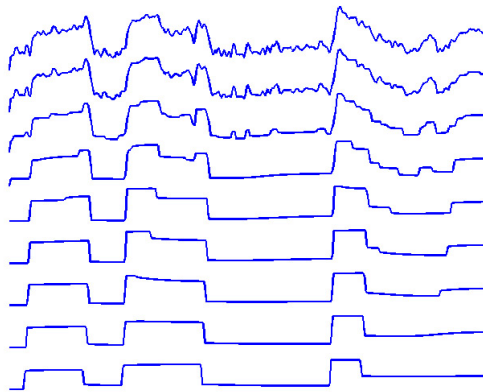


Figure 4.2: Non-linear scale space

impressive compared to the previous linear example. This time, the contours of important magnitude $|\nabla u| > \lambda$ remain sharp when the small ones are smoothed out, the inhomogeneity of the diffusion is apparent in the results. The authors have shown that edge detection based on their process outperforms the linear Canny edge detectors [33]. The diffusion seems to tend toward a step like approximation of the original image, which shows the importance of the choice of λ : too high a value would cause contours to be smoothed out, whereas too low a value would not eliminate properly all the noise. However, the theoretical foundations of the Perona and Malik diffusion reveal that the problem is not well posed and could lead to some instabilities [17]. This will be treated in Section 5.1 after looking at different interpretations of the diffusion processes.

4.3.2 Energy minimisation

A variational approach employed in image restoration can be used to unify the process and to show that anisotropic diffusion corresponds to the minimization of an energy functional. Nordstrom [49] proposed a unification of variational methods for energy minimization with the anisotropic diffusion equation as introduced by Perona and Malik [49]. Its major contribution comes from adding a reaction term which aims to keep the solution close to the original image. This reaction term leads to an optimal solution to the minimization problem, as well as getting rid of the stopping time specification.

The restoration process of an image can be explained as finding an image u which minimizes the following energy $E(u)$:

$$E(u) = \underbrace{\int_{\Omega} \Phi(|\nabla u|_2) d\Omega}_{(a)} + \beta \underbrace{\int_{\Omega} (u - u_0)^2 d\Omega}_{(b)} \quad (4.10)$$

The first part (a) of the equation corresponds to the diffusion process which will tend to a simplification of the image, whereas the second term (b) relates to the original image to control how close the result should be to the original image. β therefore plays the same role in the model as the stopping time, and choosing one or the other corresponds in the end to the same heuristic.

The minimization of an energy functional can be done by gradient descent. Using Eq. (4.10) we wish to find the minimum of $\frac{\partial u}{\partial t} = -\nabla E(u)$. The main difficulty resides in finding the expression of $\nabla E(u)$ which can be solved by using the *Euler-Lagrange Equations*.

Let f be a function of \mathbf{R}^3 in \mathbf{R} and u a function of \mathbf{R} in \mathbf{R} . Any partial derivative $\frac{\partial u}{\partial x}$ of u , will be noted u_x . The Lagrange problem tries to find an extremum of the expression:

$$E(u) = \int_{x_1}^{x_2} f(x, u, u') dx \quad \text{with: } u' = \frac{\partial u}{\partial x}$$

The theorem states that $E(u)$ has a stationary value if the Euler-Lagrange differential equation:

$$\frac{\partial f}{\partial u} - \frac{d}{dx} \frac{\partial f}{\partial u_x} = 0$$

is satisfied.

For three independent variables the Euler Lagrange differential equation generalizes to [50]:

$$\frac{\partial f}{\partial u} - \frac{d}{dx} \frac{\partial f}{\partial u_x} - \frac{d}{dy} \frac{\partial f}{\partial u_y} - \frac{d}{dz} \frac{\partial f}{\partial u_z} = 0$$

which can be simplified as:

$$\frac{\partial f}{\partial u} - \operatorname{div} \begin{pmatrix} \frac{\partial f}{\partial u_x} \\ \frac{\partial f}{\partial u_y} \\ \frac{\partial f}{\partial u_z} \end{pmatrix} = 0 \quad (4.11)$$

Using the function defined previously (4.10), we now have, for a 3D function,

$$f(x, y, z, u, u_x, u_y, u_z) = \Phi(\sqrt{(u_x^2 + u_y^2 + u_z^2)}) + \beta(u - u_0)^2 \quad (4.12)$$

We can derive the partial derivatives used in (4.11) from (4.12):

$$\begin{aligned} f_u &= 2\beta(u - u_0) \\ \frac{\partial f}{\partial u_x} &= \frac{u_x}{\sqrt{(u_x^2 + u_y^2 + u_z^2)}} \Phi'(\sqrt{(u_x^2 + u_y^2 + u_z^2)}) \\ &= \frac{u_x}{|\nabla u|} \Phi'(|\nabla u|) \\ \frac{\partial f}{\partial u_y} &= \frac{u_y}{|\nabla u|} \Phi'(|\nabla u|) \\ \frac{\partial f}{\partial u_z} &= \frac{u_z}{|\nabla u|} \Phi'(|\nabla u|) \end{aligned}$$

Using the derivatives in (4.11) the gradient descent of the energy functional can

be expressed as:

$$\begin{aligned} \nabla E(u) &= 2\beta(u - u_0) - \operatorname{div}\left(\frac{\nabla u}{|\nabla u|} \Phi'(|\nabla u|)\right) \\ \text{Hence, } \frac{\partial u}{\partial t} &= \operatorname{div}\left(\frac{\nabla u}{|\nabla u|} \Phi'(|\nabla u|)\right) - 2\beta(u - u_0) \end{aligned} \quad (4.13)$$

Comparing (4.7) with (4.13) we can see that by choosing $g(|\nabla u|) = \frac{\Phi'(|\nabla u|)}{|\nabla u|}$, the Perona and Malik diffusion tries to minimize an energy functional with the term relating to the original image (b) controlling the degree of smoothness that can be considered as acceptable.

4.3.3 Tensor diffusion

The anisotropic diffusion proposed by Perona and Malik relies on a scalar diffusivity function which is adapted to the local structure of the image. When considering the flux j Eq. (4.1), we note that it is always parallel to the gradient, i.e., $j = -g(|\nabla u|) \nabla u$. Since one might want to control completely the direction of diffusion in relation with the local structure, a tensor diffusion should be introduced to be able to rotate the flux. The need to control the direction arises from the local behavior of the Perona and Malik equation; at contours, the diffusion is inhibited, which has the consequence of not smoothing the edge and also not denoising it.

A solution to this could be to find the local direction of the gradient and smooth in the normal hyperplane, while reducing the diffusion along the gradient to preserve the edge. To this end, we construct the diffusion tensor by obtaining its eigenvectors v_i , $1 \leq i \leq 3$ according to the local structure. However, a spatial regularization is introduced when computing the eigenvectors to make the diffusion follow the edge at a higher scale. The aim of such a regularization is to make the diffusion insensitive to noise at scales lower than those specified, which might be enhanced otherwise by the diffusion. This would be particularly inconvenient at the edge where, contrary to the scalar case, the diffusion is not inhibited anymore

and noise enhancement would cause a change in the contour. The regularization is commonly the convolution with a Gaussian: $\nabla u_\sigma = \nabla(G_\sigma \star u)$. As the consequence, the eigenvectors can be derived as:

$$\begin{aligned} v_1 &\parallel \nabla u_\sigma \\ v_i &\perp \nabla u_\sigma \quad \forall i > 1 \end{aligned}$$

In order to smoothen along the edge and restrict diffusion in the perpendicular direction, we can set the corresponding eigenvalues λ_1 and λ_2 to,

$$\begin{aligned} \lambda_1 &= g(|\nabla u_\sigma|) \\ \lambda_i &= 1 \quad \forall i > 1 \end{aligned}$$

It is interesting to observe that in the general case D is a non singular matrix and the flux will not be parallel to the local gradient while $\sigma > 0$. However, when σ tends toward 0, the model tends toward the conventional Perona and Malik diffusion process. Weickert has made an extensive study of tensor diffusion [32], and terms tensor diffusion as defined above an anisotropic generalization of the Perona and Malik isotropic diffusion, which is not in harmony with the majority of the work in the image processing community.

4.4 Directional Analysis of Anisotropic Diffusion

We now present different interpretations of anisotropic diffusion in order to have a deeper understanding of the underlying process behind the diffusion equation. The idea is to present the equation driving the diffusion in a coordinate system that reflects the local structure of the image.

We first start with the 1D case to illustrate the main behavior and for the simplicity of notation. From Section 4.3.2, we have seen that the diffusivity function g from (4.7) can be changed to a flux function by doing the change: $\Phi'(x) = x g(x)$.

Eq. (4.7) can then be rewritten in the 1D case:

$$\partial_t u = \Phi''(u_x)u_{xx} \quad (4.14)$$

where u_{xx} is the second directional derivative of the image u in the x direction.

If we look at the behavior of the diffusivity function proposed in (4.9), we have $\Phi'(x) \geq 0$ for $x \leq \lambda$ and $\Phi'(x) < 0$ for $x > \lambda$. λ plays therefore the role of the contrast parameter between the low contrast areas where the flow will diffuse from higher to lower gray levels, and the high contrast areas where, inversely, the flow will diffuse from lower to higher gray levels. This property will have the worthy result of blurring small variations and enhancing strong edges.

The 1D result (4.14) can be generalized to any dimension n and was first demonstrated by Krissian in 1996 [16], though the 2D can be found in numerous works [46].

Let u be an image from \mathbf{R}^n to \mathbf{R} , Let $(\xi, e_1, \dots, e_{n-1})$ be an orthonormal basis of \mathbf{R}^n , where

$x_i = \frac{\nabla u}{|\nabla u|}$, the following property is verified with Φ as defined in Section 4.3.2:

$$\operatorname{div}\left(\Phi'(|\nabla u|)\frac{\nabla u}{|\nabla u|}\right) = \Phi''(|\nabla u|)u_{\xi\xi} + \frac{\Phi'(|\nabla u|)}{|\nabla u|} \sum_{i=1}^{n-1} u_{e_i e_i} \quad (4.15)$$

which can be simplified in 2D:

$$\operatorname{div}\left(\Phi'(|\nabla u|)\frac{\nabla u}{|\nabla u|}\right) = \Phi''(|\nabla u|)u_{\xi\xi} + \frac{\Phi'(|\nabla u|)}{|\nabla u|}u_{\eta\eta}$$

The second directional derivative in the direction of the gradient $u_{\xi\xi}$ relates to the line of maximum variation while $u_{e_i e_i}$ are the lines of constant gray values.

This result shows that the scalar diffusion as proposed in (4.7) is isotropic in the hyperplane tangent to the local isosurface, which corresponds to the hyperplane orthogonal to the local intensity gradient. By analogy with the 1D case, we can see that diffusion in the direction of the gradient has the same forward-

backward behavior between high and low gray levels areas leading to smoothing or edge enhancement depending on the ratio gradient - contrast parameter. In the orthogonal hyperplane, the diffusion is isotropic and controlled by the diffusion function $g = \frac{\Phi'(x)}{x}$.

If we wish to take tensor diffusion into consideration, the same analysis is much harder to make. Instead of Eq. (4.7), the equation to be analyzed is now:

$$\partial_t u = \operatorname{div}(D \nabla u) \tag{4.16}$$

In order to be able to analyze the directional behaviour of the matrix, we first find a basis that would help the geometric representation of the matrix. This is given by the reduction of D in a basis formed by its eigenvectors

$$\exists(\Gamma, T) \in (\mathbf{R}^3)^2 \text{ such that } D = T^t \Gamma T, \quad \text{with: } \Gamma = \begin{pmatrix} \lambda_0 & 0 & 0 \\ 0 & \lambda_1 & 0 \\ 0 & 0 & \lambda_2 \end{pmatrix}$$

The simplification of (4.16) using the eigenvector directions gives [34]

$$\partial_t u = \sum_{i=0}^2 \partial_{e_i}(\lambda_i u_{e_i}) + \lambda_i \operatorname{div}(e_i) u_{e_i} \tag{4.17}$$

We see that part of the diffusion will be along the the second directional derivatives in the direction of the eigenvectors weighted by the corresponding eigenvalues; however, there are other terms that cannot be easily simplified in the general case.

If we look at the case where D is constant over the entire image, the diffusion is then sum of the diffusions in the eigenvector directions weighted by the corresponding eigenvalues, since all the other partial derivatives are null.

However, we have seen that a constant diffusivity does not give good results, and diffusion is relevant only in the case where the diffusivity is non-homogeneous across the image since D will be changed according to the local structure of the image. We now consider the case where the eigenvector e_0 gives the orientation

of the local gradient; we have as a consequence: $D\nabla u = \lambda_0 \nabla u$, which yields the scalar anisotropic equation where λ_0 drives the diffusivity. Since the features of the image in which we are interested are the edges, we will use: $\lambda_0 = \lambda_0(u_{e_0})$. We use the framework defined above for the general tensor diffusion (4.17) and see if we can link the results to the ones derived for scalar diffusion.

Since e_0 is in the direction of the gradient we will have $u_{e_1} = 0$ and $u_{e_2} = 0$. Equation (4.17) can be simplified to:

$$\begin{aligned} \partial_t u &= \partial_{e_0}(\lambda_0 u_{e_0}) + \lambda_0 \operatorname{div}(e_0) u_{e_0} \\ &= \lambda_0 u_{e_0 e_0} + \lambda_0 (u_{e_1 e_1} + u_{e_2 e_2}) + \partial_{e_0}(\lambda_0) u_{e_0} u_{e_0 e_0} \end{aligned} \quad (4.18)$$

This result shows an equivalent solution to 4.15 for the case where D has an eigenvector in the direction of the gradient. In the general case, we choose the eigenvectors to be in the direction of the gradient and in the corresponding hyperplane as described previously. However, the regularization parameter σ used on the gradient when computing the eigenvectors will generally offset e_0 from the gradient's direction and the diffusivity $D\nabla u$ cannot be easily simplified anymore.

4.5 Summary

We have presented a brief outlook of the vast potential of diffusion techniques, from the simple physical process of heat equation to the more advanced tensor diffusion schemes. In order to find an appropriate implementation for our current problem we have to look carefully at the properties of the different techniques. We have seen that scale space theory provides a very useful framework to ensure some properties of the diffusion filter: conservation of average gray value, convergence and minimum-maximum compliance. Most importantly, energy minimization shows that the process has a physical logic, i.e., we try to reduce information in the image to keep only the features of interest which are the contours of the colon in our case. Anisotropic diffusion suits particularly well the problem; it tries to

build a piecewise image where the regions are separated by the detected contours. Moreover, the contours can be enhanced thanks to the anisotropic behavior of the filter as seen in Section 4.4. Both scalar and tensor anisotropic diffusion offer this possibility, with the latter providing more powerful restoration properties as full control of the diffusion process. We will therefore consider these two cases for implementation.

Chapter 5

Implementation of Diffusion Techniques for Noise Reduction

5.1 Choice of Functions

We have seen that, for both scalar and tensor diffusion, the diffusivity function is responsible for the global behaviour of the filter. Instead of using the functions defined by Perona and Malik, we investigate what the constraints on diffusivity are, and from there proceed to set the optimal function.

For ease of understanding, it is preferable to use the same notations as in the directional interpretation of the diffusion equation (4.15):

$$\partial_t u = \Phi''(|\nabla u|)u_{\xi\xi} + \frac{\Phi'(|\nabla u|)}{|\nabla u|} \sum_{i=1}^{n-1} u_{e_i e_i}$$

To ensure convergence of the energy minimization, a *stability condition* requires the convexity of the energy, which leads to a unique global minimum. This can be formulated mathematically by

$$\Phi''(|\nabla u|) \geq 0 \tag{5.1}$$

$$\Phi'(|\nabla u|) \geq 0 \tag{5.2}$$

Table 5.1: Diffusivity functions

Name	Function $\Phi'(x)/x$	Stability		Restoration	
		5.1	5.2	5.3	5.4
Heat transfer	1	✓	✓		✓
Perona & Malik,1 [33]	$e^{-(\frac{x}{\lambda})^2}$		✓		✓
Perona & Malik, 2 [33]	$\frac{1}{1+(\frac{x}{\lambda})^2}$		✓		✓
Charbonnier [51]	$(1 + (\frac{x}{\lambda})^2)^{-\frac{1}{2}}$	✓	✓	✓	✓
Black [52]	$\begin{cases} (1 - (\frac{x}{\lambda})^2)^2 & \text{for } x < \lambda \\ 0 & \text{elsewhere} \end{cases}$		✓		✓
Weickert [32]	$\begin{cases} 1 - e^{\frac{-C_m}{(x/\lambda)^m}} & \text{for } x > 0 \\ 1 & \text{elsewhere} \end{cases}$		✓	✓	✓

The *restoration property* expresses the logical behaviour of the filter:

- For high gradient areas the diffusion must only occur in the orthogonal hyperplane to the gradient direction for both edge and contrast enhancement. However no diffusion should occur in the direction of the gradient.
- For homogeneous areas corresponding to $|\nabla u|$ near to 0, the diffusion filter must have an isotropic reaction.

For high gradient areas we will therefore look for functions that ensure:

$$\begin{aligned} \lim_{x \rightarrow \infty} \Phi''(x) &= 0 \\ \lim_{x \rightarrow \infty} \frac{\Phi'(x)}{x} &= 0 \\ \lim_{x \rightarrow \infty} \frac{\Phi''(x)}{\Phi'(x)/x} &= 0 \end{aligned} \quad (5.3)$$

On the contrary, in homogeneous regions we will seek to let diffusion flow:

$$\lim_{x \rightarrow 0} \Phi''(x) = \lim_{x \rightarrow 0} \frac{\Phi'(x)}{x} \geq 0 \quad (5.4)$$

We look at the different functions that have been proposed in the literature to see what the possibilities when defining the diffusivity function are.

We study 6 models which are presented in Table 5.1.

- The first model corresponds to the heat diffusion equation, with isotropic homogeneous diffusion.
- The following two models are the ones proposed by Perona and Malik, at the time when the complete diffusion framework had not been established; hence, we can see that the stability and restoration constraints are not all fulfilled.
- Convex functions were proposed by Charbonnier to deal with the instability problems.
- The last two models are based on more recent work by Weickert and Black. With the background of the diffusion equation better established, they focus on some characteristics of the functions with less emphasis on the constraints mentioned above. Black's model is based on the Tukey function. Weickert's model is defined such that the flow $\Phi'(x)$ is increasing for $x < \lambda$ and decreasing for $x \geq \lambda$. m sets the slope of the model, and a usual compromise is $m = 4$ as used in Figure 5.1.

The curves are presented in Figure 5.1. λ is set at 10 for all the models.

We can see that the global shape of the flow functions $\Phi'(x)$ is very close for all functions, which is expected with the numerous constraints. However some small differences lead to major changes in the diffusion equation. When x increases, all the diffusivity coefficients tend toward 0; however, this value is only reached by the Black function. For all the other models this means that diffusion will still occur even for high gradients, whereas in the Black model, for gradients higher than a specified value λ , the diffusion will be completely stopped. Only the Black model can therefore ultimately lead to a piecewise steady state result, but might have more difficulties when confronted with highly noised images. We note that in the Black model, λ here sets the highest value after which the diffusion will be stopped, while it plays the role of a contrast parameter in the other models. The

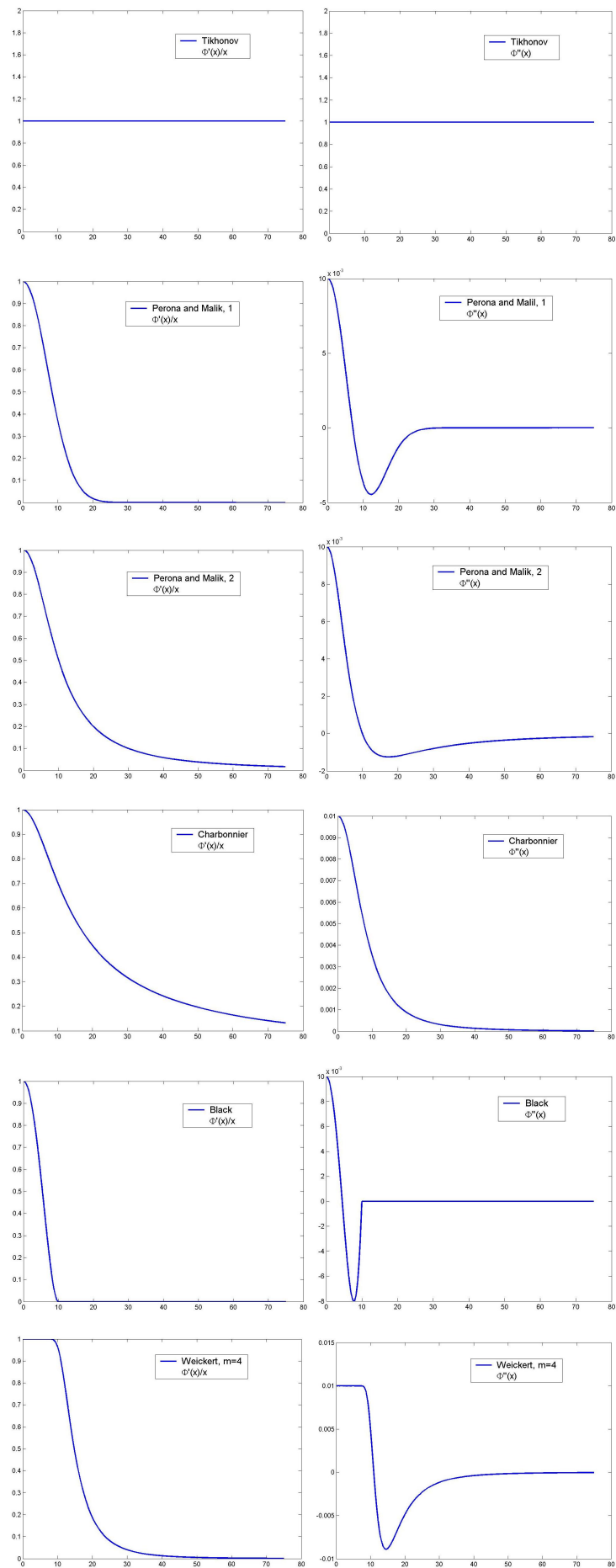


Figure 5.1: Diffusivity functions

contrast parameter in that case is internal to the Black model. Other differences are for example the slopes of the flow function or its decreasing rate. The function defined by Weickert has the interesting property to be nearly flat up to λ where it then drops sharply, with the possibility of controlling the slope with m .

An important feature lies in the coefficient $\Phi''(x)$, which controls the diffusion in the gradient direction as seen in Eq. 4.15. The models can be classified into two groups: those which have a strictly positive coefficient and those whose coefficient can take negative values. Table 5.1 shows us that the two Perona and Malik models, as well as the ones defined by Black and Weickert, all fall into the second category. If $\Phi''(x)$ can take negative values, the convexity constraint will not be satisfied anymore, leading to possible instabilities in the process. When Φ'' is negative the gradient is enhanced instead of being diffused, leading to a possibly better contrast which seems a very interesting feature in the context of noise reduction and contour preservation. Nevertheless this can be assimilated to the inverse heat diffusion which is well known to be ill-posed, and discontinuities introduced by noise can be increased. To ensure convergence of the process regularization needs to be introduced.

5.2 Regularization

Numerous numerical simulations of the ill posed Perona and Malik process have shown that in fact the implementation of the process works much better than expected from theory. The usually impressive results of an ill-posed problem has been therefore called the *Perona and Malik paradox*.

Discretization plays an important role in regularizing the equation, and although formal explanations have not been established in the general case, current research points to the same direction; namely, discretization yields a regularization [53]. The finer the discretization the less regularization is provided and the dangers of instability are more significant. Among the artefacts that can occur, stair-casing is the most frequent one, in which a smooth edge can be changed into a staircase like

function. Weickert and Benhamouda have even proved that standard spatial finite difference discretization transforms a Perona and Malik ill-posed problem into a well-posed system of nonlinear ordinary differential equations (ODEs) which is monotonically preserving under explicit time discretization [54]. No real instability can thus occur other than the staircasing effect.

To become more independent of the implementation of the process, it comes to mind to try to introduce a regularization in the process itself to stabilize it and ignore the unreliable and imprecise implicit regularization.

Catte *et al.* have introduced a new model where the only change lies in the gradient used in the diffusivity function [17]. A smoothed gradient $\nabla u_\sigma = \nabla(G_\sigma \star u)$ is used where G_σ can be any smoothing kernel and for which the Gaussian is used commonly. The diffusion equation can thus be written as

$$\partial_t u = \operatorname{div}(g(|\nabla u_\sigma|) \cdot \nabla u)$$

With this simple modification, they prove the existence and uniqueness of a solution for an initial image and its corresponding set of parameters.

It is interesting to note that Weickert's tensor diffusion is based on this regularization of the scalar diffusion, and can even be considered as a particular regularization of the general scalar anisotropic diffusion equation with the regularizing parameter σ controlling the smoothness of the contours. This latter property is a practical consequence of spatial regularizations; they make the diffusion filter insensitive to noise at a scale smaller than σ both in the tensor and scalar case.

Many other regularization schemes can be found, both in the spatial domain, where the schemes work mainly on scale space features, as well as in the temporal domain with the introduction of a relaxation time in the diffusivity, for instance.

5.3 Numerical and Discrete Schemes

Practical experiments require the continuous differential equation to be discretized both spatially and temporally. Various choices of discretization are possible and this is a decisive factor in the stability of the process as well as the speed of computation.

We can first show the path from the continuous model to a discrete one via a semi discrete model which helps in the understanding of how the characteristics of the scale space are controlled in the process. The scale space theory established in the continuous framework also has to be adapted into a discrete environment to ensure that the discrete process will have the exact same properties as the continuous one. An exhaustive study can be found in [32]. Table 5.2 summarizes the requirements needed to prove the major properties: well-posedness of the problem, conservation of the average gray value, maximum-minimum property, Lyapounov sequence ensuring smoothing, and convergence to a steady state.

- Continuous model:

$$\begin{cases} u(x, 0) = u_0 & \text{on } \mathbf{R}^3 \\ \partial_t u = \operatorname{div}(D \cdot \nabla u) & \text{on } \mathbf{R}^3 \times [0, \infty[\end{cases} \quad (5.5)$$

- Semi discrete model

$$\begin{cases} u(0) = u_0 \\ \frac{du}{dt} = A(u)u \end{cases} \quad (5.6)$$

- Discrete model

$$\begin{cases} u^0 = u_0 \\ u^{k+1} = Q(u^k)u^k \end{cases} \quad (5.7)$$

Since the spatial discretization is inherent in digital images, the step from the fully continuous model to the semi-discrete one is fairly natural. The pixel structure assuring a discretization on a fixed rectangular grid is very well suited to finite differences schemes which will be used for the approximation of the diffu-

Table 5.2: Discretization models

Requirement	Continuous Model	Semi-discrete Model	Discrete Model
Smoothness	$D \in C^\infty$	A Lipschitz continuous	Q continuous
Symmetry	D symmetric	A Symmetric	Q symmetric
Conservation	divergence form, reflective boundary condition	column sums null	unitary column sums
Non-negativity	positive semi definite matrix	non-negativity of A	non-negativity of Q
Connectivity	D uniform positive definite	irreducibility of A	irreducibility of Q positive diagonal

sivity. This is expressed in the above equation with the differentiation matrix A . However, temporal discretization is not as straight forward and a numerical scheme giving an example of how to pass from the semi discrete to the discrete model is presented in below.

The temporal discretization of the semi-discrete model 5.6 can be done with the usual explicit scheme. Let u^k represent the image u at time t and u^{k+1} at time $t + \tau$. The differentiation matrix A is here calculated at step k to approximate the temporal derivative $\frac{du}{dt}$:

$$\begin{cases} u^0 = u_0 \\ \frac{u^{k+1} - u^k}{\tau} = A(u^k)u^k \end{cases} \quad (5.8)$$

This corresponds to the discrete model with $Q(u^k) = I + \tau A(u^k)$. This scheme is the simplest one to implement and can be used with relatively big images since the computation is direct. Yet, to ensure stability of the process the time step τ has to be very small:

$$\tau \leq \frac{1}{\max_{i \in J} |a_{ii}(u^k)|} \leq \frac{1}{2n}$$

with n being the dimension of the images.

To circumvent this problem, it is tempting to use the values at time $k + 1$ to

estimate the differentiation matrix and apply it consequently at time $k + 1$:

$$\begin{cases} u^0 = u_0 \\ \frac{u^{k+1} - u^k}{\tau} = A(u^{k+1})u^{k+1} \end{cases} \quad (5.9)$$

This scheme is called the implicit scheme because the computations are done on the basis of a smoother future image, rather than using the image itself to get to an unknown future one. The stability of the process is considerably increased, but the system is now nonlinear in u^{k+1} and hence much more difficult to solve and computationally not viable for large images.

The idea to solve the nonlinearity is to use time k to control the diffusion but to apply it at another time, in the future. A β semi-implicit scheme is defined in that objective:

$$\begin{cases} u^0 = u_0 \\ \frac{u^{k+1} - u^k}{\tau} = A(u^k)(\beta u^{k+1} + (1 - \beta)u^k) \end{cases} \quad (5.10)$$

Hence,

$$u^{k+1} = (I - \tau\beta A(u^k))^{-1}(i + \tau(1 - \beta)A(u^k))u^k \quad (5.11)$$

For all β , the scheme is now linear in u^k and can be reduced to a linear system which comprises an inversion. The complexity of the linear system depends on the form of the inverse to be computed. The value $\beta = 0$ would lead to the direct explicit scheme, whereas the value $\beta = 1$ gives a true semi-implicit scheme, in which the diffusion is calculated at time k but applied at time $k + 1$. The stability is also much greater since it is stable for all time steps satisfying:

$$\tau \leq \frac{1}{(1 - \beta) \max_{i \in J} |a_{ii}(u_k)|} \quad (5.12)$$

For the case where $\beta = 1$ the scheme will be stable unconditionally of the time step. The properties from the scale space theory as defined in Table 5.2 will also be ensured provided A satisfies the requirements of the semi discrete model.

Now that we are not limited by small time steps to approximate the diffusivity, we would also like the model to be computationally efficient. The inverse which needs to be calculated is a major drawback, and a simplification has been proposed in [55] with the additive operator splitting (AOS) scheme. This novel scheme is based on the semi-implicit scheme ($\beta = 1$) and separates the coordinates to treat them independently as 1D processes. Letting n be the dimension of the images, we can write:

$$A(u^k) = \sum_{l=1}^n A_l(u^k) \quad (5.13)$$

with A_l being the differentiation matrix along the l th dimension. The semi-implicit scheme can therefore be written as

$$u^{k+1} = (I - \tau \sum_{l=1}^n A_l(u^k))^{-1} u^k \quad (5.14)$$

The approximation made with the AOS scheme yields:

$$u^{k+1} = \frac{1}{n} \sum_{l=1}^n (I - n\tau A_l(u^k))^{-1} u^k \quad (5.15)$$

A Taylor expansion shows that the order of approximation of the AOS scheme is the same as the semi-implicit one (first order). Now that the matrix A is the sum of matrices working on 1D processes, we can see that we still have to invert some matrices in order to be able to get the value at a new time. The trick is that since we are dealing with one dimensional processes, the matrix can be arranged so as to be working on tridiagonal matrices. The inversion of such matrices can be done much more efficiently than a standard inversion scheme, giving the true strength of the technique in comparison to classical semi-implicit schemes.

The implementation of the AOS scheme is easily done in the scalar diffusion case, where the differentiation matrices A can be obtained and separated without much difficulty, and it creates a discrete scale space as defined in Table 5.2 with all the corresponding properties.

However, the tensor diffusion case is much more difficult to implement practically. The main difficulty is to split the 3D diffusion tensor D correctly into 1D diffusivities to fill the matrices A_l . In order to obtain the properties of the diffusion filter, such as maximum–minimum principle, stability, wellposedness etc., we require each directional diffusivity to fulfill some constraints. The complexity of such an implementation is such that it will not be dealt with in this work and tensor diffusion experiments will be done using a classic non-optimal explicit scheme. More details on AOS schemes in tensor diffusion filters can be found in [56].

The freedom to select a larger time step τ means that fewer iterations are needed to reach the same diffusion time, and the algorithm becomes faster. Though long step times carry the drawback of weakening the precision of the filtering by doing larger approximations, Weickert has shown that under normal considerations it is about 11 times more efficient than the stable explicit scheme [55]. Table 5.3 summarizes the characteristics of the different techniques.

caption Numerical schemes

Technique	Formula	stability	cost	Efficiency
Explicit	$u^{k+1} = (I + \tau A(u^k))u^k$	low	low	low
β Semi-implicit	$u^{k+1} = (I + (1 - \beta)\tau A(u^k)) (I - \beta\tau A(u^k))^{-1} u^k$	high	high	moderate
AOS	$u^{k+1} = \frac{1}{n} \sum_{l=1}^n (I - n\tau A_l(u^k))^{-1} u^k$	high	low	high
Implicit	nonlinear	high	very high	low

5.4 Choice of Parameters

With the framework having been defined above, the chosen functions and parameters for the experiments are presented below.

Both the scalar and tensor-based diffusion will be compared to determine the method with higher restoration properties. For ease of comparison, the same function will be chosen in the gradient direction for both the scalar and tensor-based schemes. For the latter, the diffusion will be set to 1 in the orthogonal hyperplane to the gradient, which should help edge restoration as described previously.

Functions: The preferred function to be retained is the one defined by Weickert, because of its enhancement properties and interesting characteristics (flat diffusivity up to λ , slope that can be controlled). Since one of the stability requirements is not fulfilled (Table 5.1), the Gaussian regularization on the gradient will also be taken into account in the process. The much desired edge enhancement capabilities of Weickert's function justifies totally the choice not to take a fully compliant function. The parameter m enables us to control the slope of the diffusion function, and the choice of the parameter lies in the compromise between stability and edge enhancement. The retained value $m = 4$ is a reasonable choice under a regularized process and gives good enhancement of edges. The implementation with Weickert's function will be tested against other functions to confirm the efficiency of the chosen scheme.

Numerical scheme: The efficiency of the AOS scheme offers very good stability independently of the step time and makes it preferable compared to other possibilities. Since it is based on the inversion of tridiagonal matrices, one has to make sure that this is done efficiently to ensure the lowest computational cost possible. The *Thomas algorithm* is perfectly suited to the task since it manages to invert those matrices with a computational cost proportional to the number of pixels and the dimension.

For the tensor-based diffusion where the AOS scheme cannot be easily implemented, the direct explicit scheme will be used.

Time step: The stability of the AOS scheme is independent of the time step. This gives us the freedom to select a larger τ so that the number of iterations is globally reduced and the algorithm becomes faster. The AOS scheme also ensures that for all τ the diffusion process can be assimilated to a scale space transformation with all the corresponding properties. However step times that are too large would weaken the filtering effect of the the diffusion filter and only yield a rough approximation of the ideal continuous result. The choice of time step τ is therefore a compromise between efficiency and

accuracy. For the explicit scheme, the step time is set as to ensure stability as shown earlier.

Diffusion time: The total diffusion time controls the degree of simplification desired for the smoothed image. This is a very tricky part and it is subject to many never ending discussions. As long as convergence is ensured, we can try out different diffusion times and choose the most appropriate one for the current problem. Very long diffusion times will tend toward segmentation like results, and one has to take into consideration whether this is the kind of result that is desired with such an implementation or whether it is more oriented toward image denoising. For the experiments we opt to show the evolution of the scale space along with the diffusion time, to allow comparisons and to give us an insight into the problem.

Contrast parameter: All the diffusivity functions have a contrast parameter λ which acts as a contour detection. If the ratio gradient - contrast parameter is large, it is synonymous to an edge, and diffusion should be restrained in the orthogonal direction of the edge. This parameter has to be set with care; if it is too low the restoration of the image would be close to null, if it is too high some edges would be smoothed out. This will be verified quantitatively in Section 5.5.1. To this end we will try to set the contrast parameter statistically. Since we only wish to keep the higher gradients we can set it as a quantile in the cumulative histogram of the image absolute gradients. Analysis of the images has shown that the 40% percentile yields good results. This may seem quite low for images which are supposed to highlight the strong contours of the colon predominantly, however it comes from the characteristics of the datasets. They are large and include many other medical features other than the colon; the kidneys, bottom part of the liver, small intestine and even the skin interface are also depicted with good contrast, which increases the proportion of high gradients in the cumulative histogram.

5.5 Results and Comparison

5.5.1 Analysis of parameters and diffusion techniques

We first wish to do a quantitative analysis of the diffusion process under different implementations and parameters. We would like to be sure that the theoretical properties seen previously are verified, and be able to set the parameters optimally for a specific problem.

To meet the above objectives we create a test image (Fig. 5.2) with features that we are likely to encounter in the real dataset, namely, thin structures. Sharp corners are also present in the image so that there is an easy way of investigating the preciseness of contours. Gaussian and speckle noise are added to the test image to model a noisy dataset. The Gaussian added is of mean zero and standard deviation 0.4 times the intensity range in the image while the speckle noise is controlled by

$$u = u + \eta u$$

with η being uniformly distributed of mean 0 and standard deviation 0.1. the Gaussian noise is characteristic of natural images whereas speckle noise is here to distort more significantly the images. We end up with a relatively noisy image where noise reduction will be hard to perform. The SNR is measured using

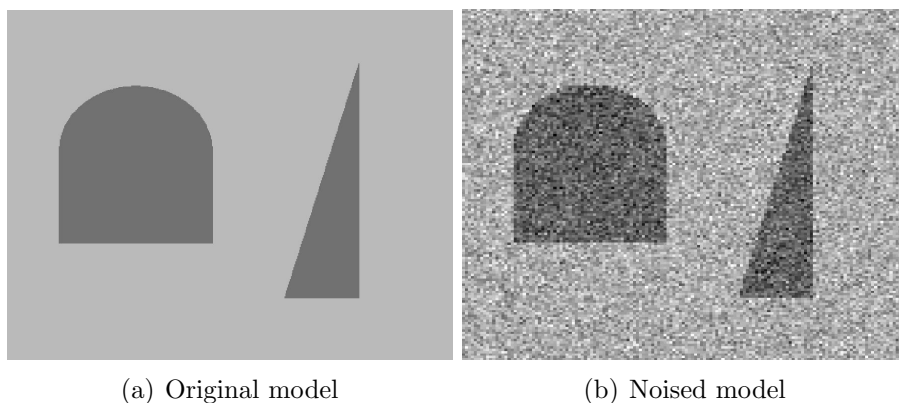


Figure 5.2: Test image

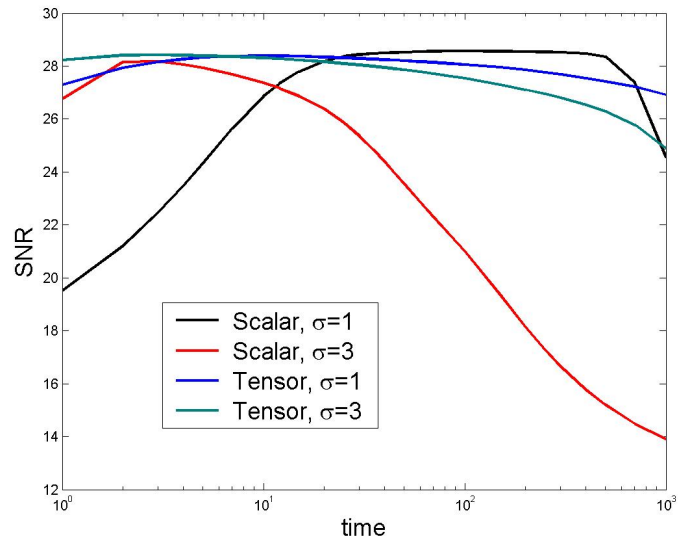
$$SNR(dB) = 10 \log_{10}\left(\frac{P_{signal}}{P_{noise}}\right) = 20 \log_{10}\left(\frac{A_{signal}}{A_{noise}}\right)$$

This gives an SNR of 18.97 for the noisy image.

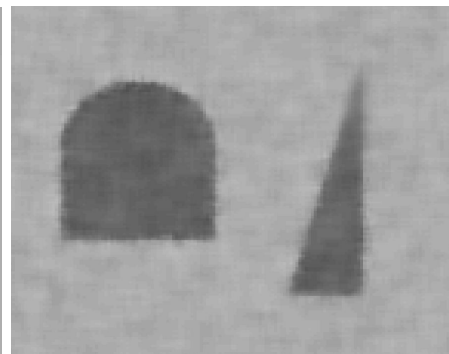
We first check the influence of the type of diffusion process. Since we have seen the limitations of linear scale space, we will focus on the two types of anisotropic diffusion processes, namely scalar and tensor diffusion. The same diffusivity function is chosen for the two schemes and the parameters are set identically. Two values of for the regularization parameter ($\sigma = 1$ and $\sigma = 3$) are tested in order to verify that the experiment is not corrupt by this parameter.

The SNR curves are represented as a function of the diffusion time, and the result corresponding to the best SNR for each curve is represented underneath, (Fig. 5.3). A brief analysis of the curves show that they all have the same general aspect, although their maxima are reached at different times in the scale space. This would correspond to a faster scale space behaviour for the tensor scheme which is not surprising because the flow is much stronger than in the scalar case since in the hyperplane normal to the gradient the diffusion is set at 1 so that it flow freely.

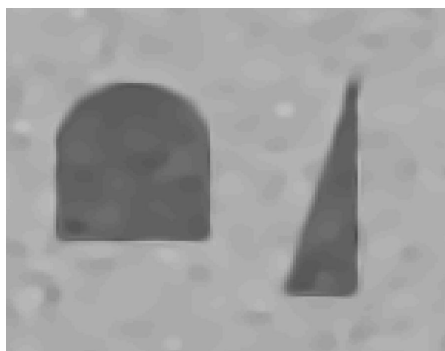
We also notice that once each curve reaches its maximum, the SNR decreases. This is caused by over-diffusion, when the diffusion starts to affect the contours. As anticipated, it happens much more quickly for tensor diffusion. This is further highlighted by the images which show very different results; while edges are very well defined in the scalar case with a low regularization, for the equivalent case with a tensor diffusivity, there is still some noise in the homogeneous regions. It shows that complete noise reduction can only be obtained at the expense of a change in the contours; the corners are not as sharp anymore but start to be rounded, and the top part of the thin structure is not well defined anymore. On the positive side, the tensor scheme offers higher edge restoration; when the edges are badly affected by noise, scalar diffusion has not managed to restore straight edges when tensor based diffusion has.



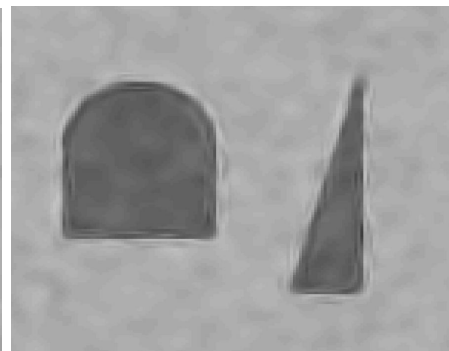
(b) Scalar Diffusion,
 $\sigma = 1$, $t=100$, SNR=28.67



(c) Scalar Diffusion,
 $\sigma = 3$, $t=5$, SNR=28.18



(d) Tensor Diffusion,
 $\sigma = 1$, $t=12$, SNR=28.38



(e) Tensor Diffusion,
 $\sigma = 3$, $t=3$, SNR=28.67

Figure 5.3: Analysis of the diffusion scheme

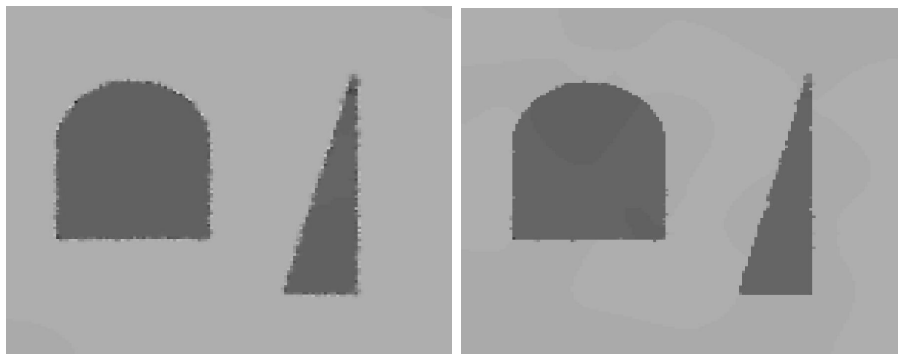
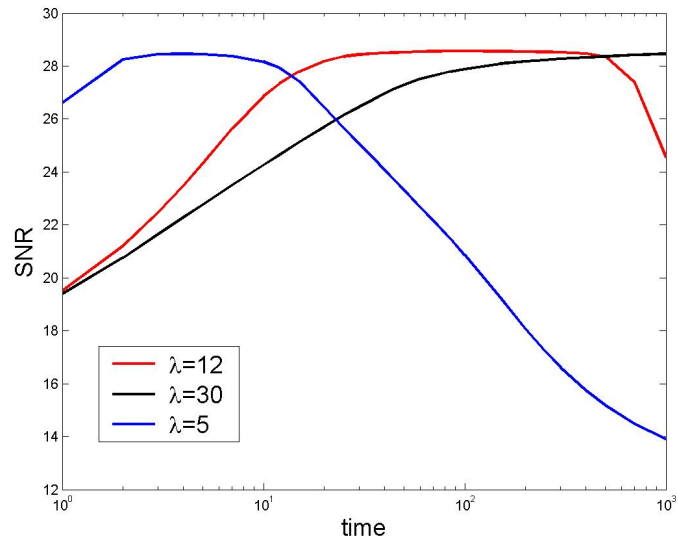
If we look at the influence of the regularization parameter we can see that it does have a negative influence on the process. With tensor diffusion, the edges are a bit more rounded and less precise, while with scalar diffusion the edges get smoothed and the reduced restoration properties of the process does not manage to get them back.

We now examine the influence of the contrast parameter. We keep the process that yield the best results previously, namely, scalar diffusion with a regularization parameter of 1, and do experiments by changing the contrast parameter. The results are presented in the same manner in Fig. 5.4.

The results are in agreement with the theoretical results. When the contrast parameter is set low, the process has difficulty removing the noise. We observe that after a very long time, the edges are still extremely noisy. Since the diffusion is reduced significantly at the edges, an extremely long time is required to enhance the edge. The background which has been perfectly restored shows however that $\lambda = 5$ is a value high enough to smoothen the edge if there is no information in the image. On the opposite, a high value of λ does not recognize edges anymore, and the diffusion is not restrained anywhere. Careful examination shows that the edges are starting to get diffused in some areas, and this image corresponds to the highest SNR because the diffusion would only affect the image even more as time increases.

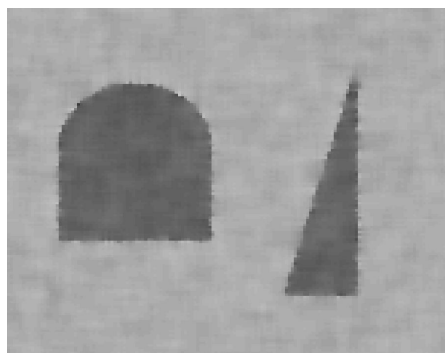
Lastly we check whether the desired properties of Weickert's function hold their theoretical promises in the experiments. We use Charbonnier's fully compliant function as well as the heat equation diffusion to verify that there is a gain in choosing the diffusivity function carefully. All the other parameters are set identically for ease of comparison.

From the best case images (Fig. 5.5) the edge enhancing capacity of Weickert's function proves to be very efficient. Looking at the SNR curves, it seems that the diffusion process is not effective for the two other models because their SNR curves drop right after a few iterations. This is because the models do not have



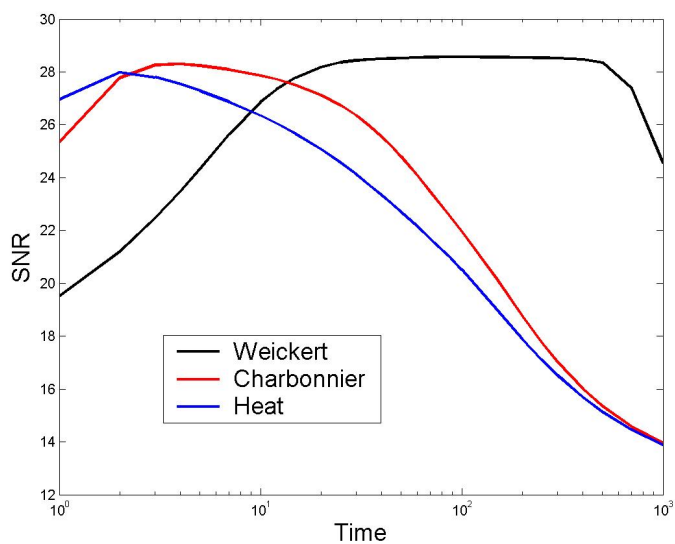
(b) Scalar Diffusion,
 $\lambda = 5$, $t=1000$, SNR=28.46

(c) Scalar Diffusion,
 $\lambda = 12$, $t=100$, SNR=28.67

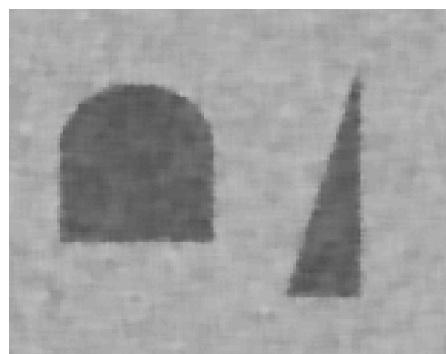


(d) Scalar Diffusion,
 $\lambda = 20$, $t=4$, SNR=28.44

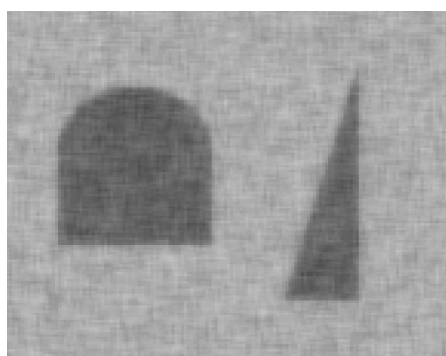
Figure 5.4: Influence of the contrast parameter



(b) Scalar Diffusion, Weickert, $t = 100$, SNR=28.67



(c) Scalar Diffusion, Charbonnier, $t = 4$, SNR=28.29



(d) Scalar Diffusion, Heat, $t = 2$, SNR=27.99

Figure 5.5: Influence of the diffusivity function

edge enhancing capacity and the noise is removed at the expense of smoothing the edge. However, we observe that diffusion based on Charbonnier's function achieves better results than heat diffusion. This is because Charbonnier's model reduces the diffusion at edges. Nonetheless, the reduction is not sufficient for images with a high noise level.

From these experiments we see that the parameters have a tremendous influence over the diffusion process. The results presented here show that the experiments are in accordance with the theoretical results established. It is not clear whether the scalar or tensor scheme is preferred. The first one aims at better localization of the edges but offers lower restoration than tensor based diffusion. Both schemes will be tried out on real images.

5.5.2 Application to MR abdominal images

The datasets used for the experiments come directly from the MR acquisition protocol. Their original size is $512 \times 512 \times 80$ along the 3 spatial dimensions with resolutions of respectively 1mm, 1mm and 2mms. They are therefore resampled before processing with bicubic interpolation to give isotropic datasets of size $512 \times 512 \times 160$. A time step of 10 is chosen for the scalar anisotropic diffusion under AOS scheme, as a compromise between efficiency and accuracy. For the tensor case, the step size is set at 0.1 as required for stability of the explicit scheme. A regularization $\sigma = 1$ is applied to both implementations.

The total computation time is about one hour for the 3D AOS scheme implemented in Matlab on a single core Pentium IV 3.0 GHz PC with 1GB of RAM memory running on Windows XP. Using multiple cores and increasing the memory should reduce significantly the processing time. The large size of the dataset justifies the high memory requirements to achieve acceptable processing time.

The results of a slice of the dataset for increasing diffusion times are presented in Fig. 5.6 with the same results zoomed in on a detail proposed in Fig. 5.7.

We observe that the tensor based process has a faster scale space behaviour

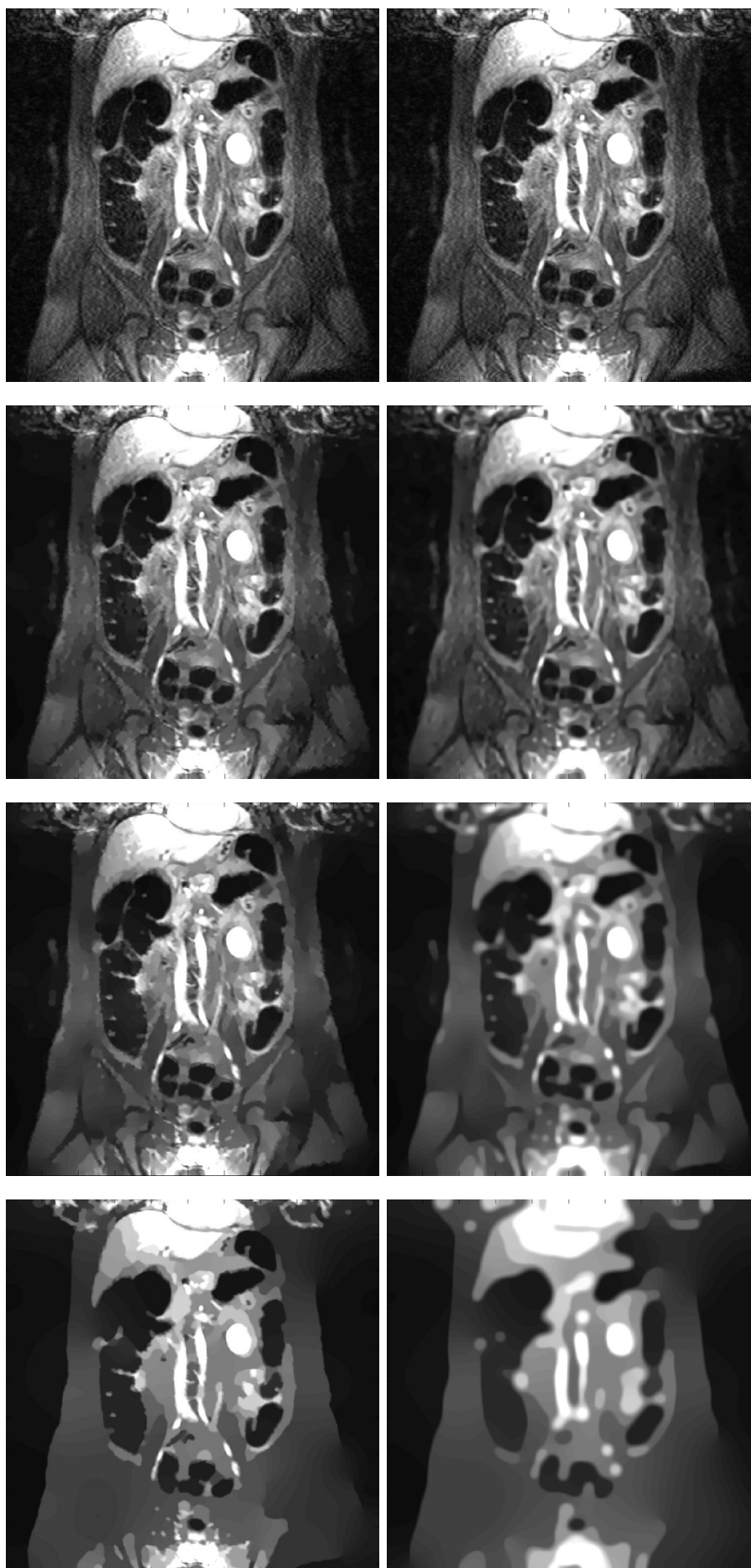


Figure 5.6: Diffusion Scale spaces. Left column: scalar anisotropic diffusion. Right column: tensor anisotropic diffusion, from top to bottom $t = 0, 10, 100, 1000$

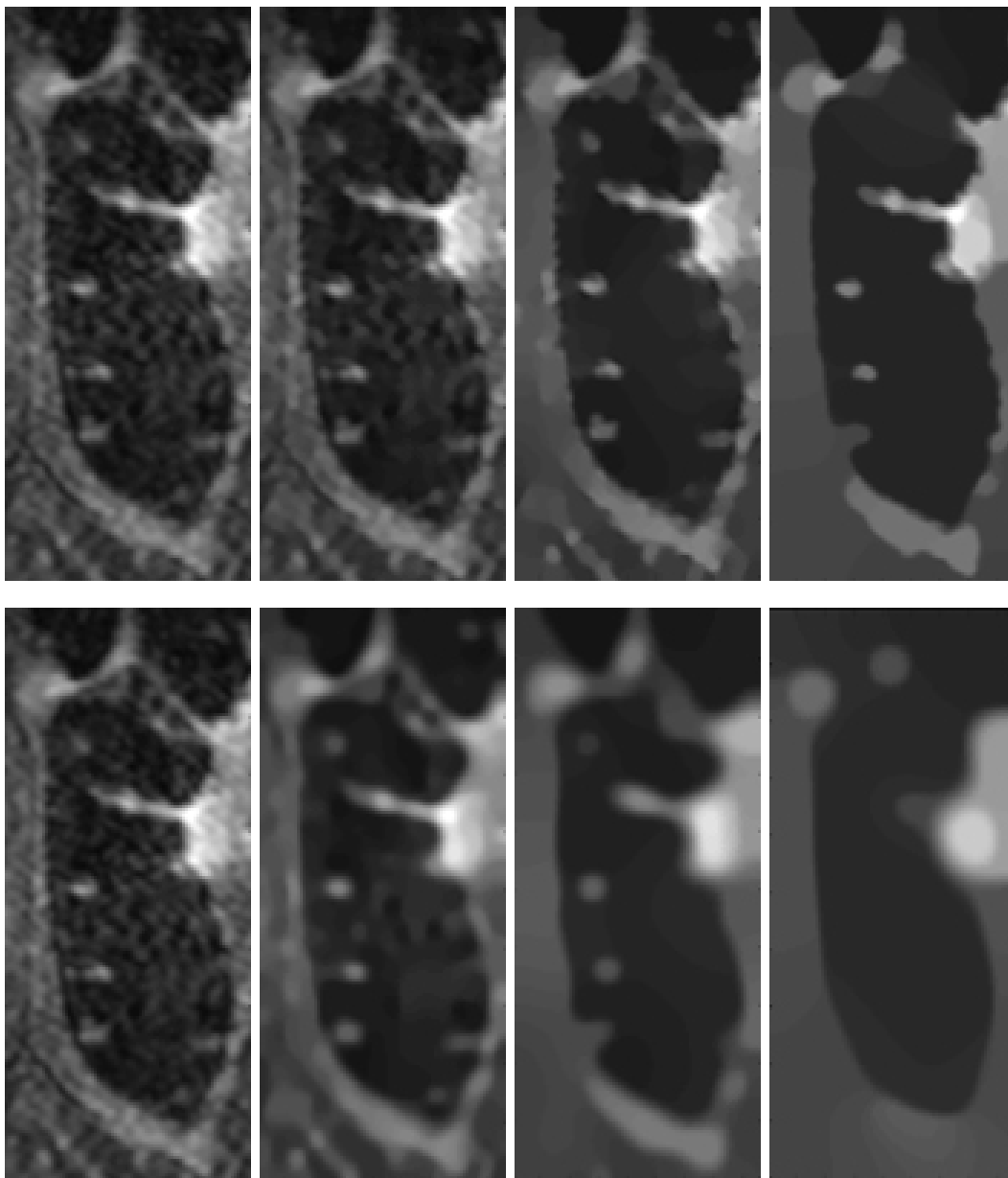


Figure 5.7: Diffusion Scale spaces, zoom of Fig. 5.6. Top row: scalar anisotropic diffusion. Bottom row: tensor anisotropic diffusion, from left to right $t = 0, 10, 100, 1000$

than the scalar one, as seen on the test image. The diffusion along the edge also creates a rounding effect which causes sharp corners to be turned into round shapes, creating a flow-like effect. Small structures are eliminated in favor of elongated boundaries. This is very inconvenient in our current problem because it would smoothen polyps (by making them lose their original shape as they appear flatter), as well as making them appear smaller. The texture of the colon wall, which is not perfectly smooth and can even be a bit rough in case of tumors, would also be totally lost with that process. This behaviour is not surprising as it was one of the main findings of Weickert [32] on the restoration properties of tensor based anisotropic diffusion.

On the contrary, the scalar diffusion exhibits a very slow scale space evolution. The edges stay very well localized and structures stay very well defined for a reasonably long time provided they have a scale and contrast sufficient not to be considered as noise from the beginning. The noise reduction potential of scalar anisotropic diffusion is however lower on the edges. While the diffusion along the edges tries to yield smooth edges as a major feature, the scalar scheme protects the boundaries as much as possible from any major change, thus weakening correspondingly the noise reduction properties on the edges.

Both processes are also capable of enhancing boundaries, as can be seen in Fig. 5.7 where some smooth edges become better defined after some time, and the average gray levels are conserved in the image as shown theoretically.

The evolution of both scale spaces shows a tendency to create piecewise regions in the images, delimited by strong contours that are enhanced and with internal details and noise that are smoothed out. This is well suited as a pre-segmentation step where only the most important regions will be kept from the original image. Careful analysis shows that the predominant features are slightly different for the two schemes: while tensor-based anisotropic diffusion tries to conserve the global aspect of the most representative regions the longest at the cost of localization and precision, the scalar scheme gives preference to accuracy over the global perception

of the region.

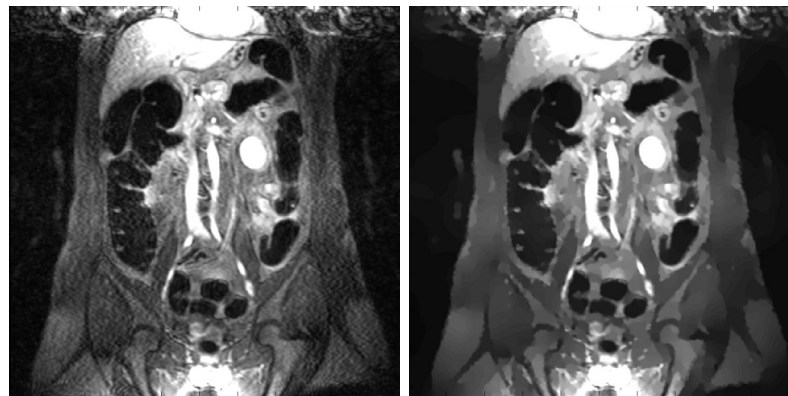
The scale parameter t reveals here its full importance: it creates a complete family of segmentation-like images, and not a single result to which the diffusion tends as the diffusion time increases. Setting t corresponds therefore to choosing at which level of hierarchy in the scale space we want to stop the process. From Fig. 5.6 we can set the parameter t with relative ease in the scalar diffusion experiments: $t = 1000$ is obviously too long since we can see that some structures have already disappeared; while at $t = 10$ the image is still heavily corrupted by noise, that we would like to reduce further. In between the two, $t = 100$ offers precise and neat contours with a low noise level inside the regions, which are appropriate features to continue onto a segmentation process.

With clear edges, the scalar scheme yields manifestly superior results for the present purpose. We should not forget that the global objective is to obtain a model of the colon for clinical analysis so has to be able to detect polyps and tumors as small as a few millimeters. In consequence, we try to keep as many details as possible on the colon wall. The tensor diffusion process smooths excessively the boundary and it corresponds to significant loss of information which cannot be tolerated here.

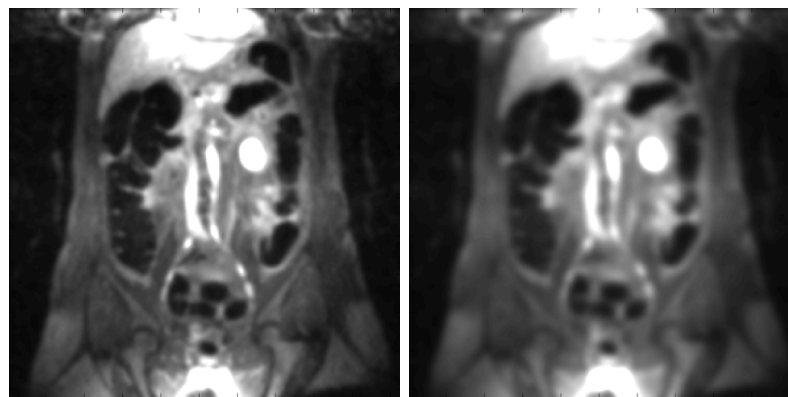
5.5.3 Comparison with other noise removal techniques

We test the anisotropic diffusion techniques proposed above against other classic noise reduction techniques to assess the strength of our implementation. Only a qualitative comparison will be provided because qualitative results established on SNR computation does not represent very efficiently all the features we are looking for in the results. Moreover the results are clear enough for a qualitative comparison. The implementation retained for comparison is the one giving the better results for our objective, i.e., the scalar anisotropic diffusion with a total diffusion time equal to 100.

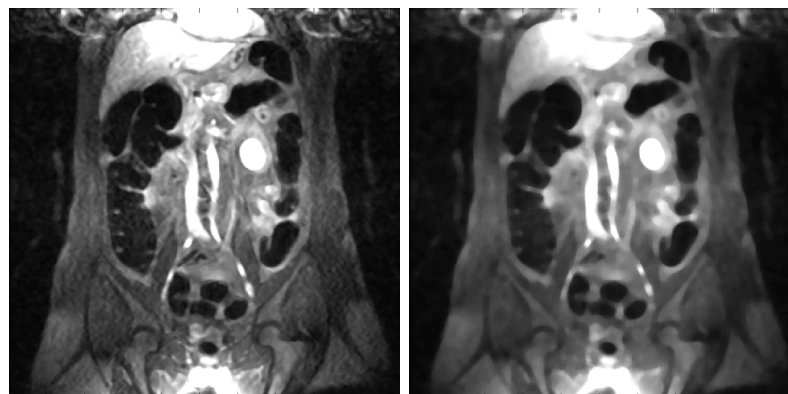
The quality of the noise reduction proposed is clearly unrivaled by the classic



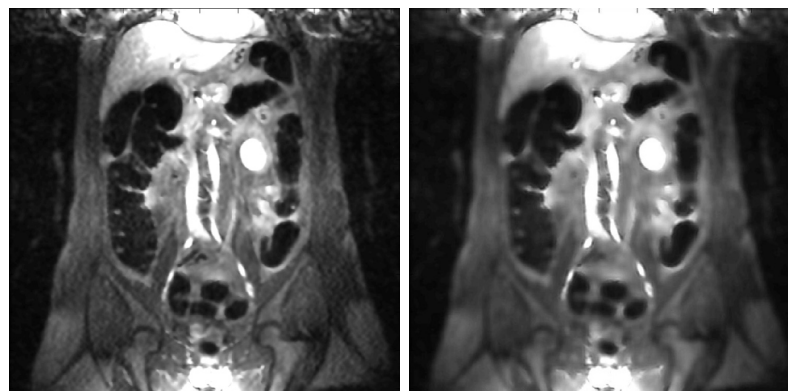
(a) Scalar Anisotropic Diffusion, $t = 0$ (b) Scalar Anisotropic Diffusion, $t = 100$



(c) Gaussian smoothing, $\sigma = 3$ (d) Gaussian smoothing, $\sigma = 5$



(e) Median filtering, $5 \times 5 \times 5$ neighborhood (f) Median filtering, $10 \times 10 \times 10$ neighborhood



(g) Wiener filtering, $5 \times 5 \times 5$ neighborhood (h) Wiener filtering, $10 \times 10 \times 10$ neighborhood

Figure 5.8: Comparison of noise reduction techniques

techniques shown in Figure 5.8.

As shown theoretically, Gaussian filtering has a strong noise reduction potential but blurs the features very quickly. Since we need to keep all possible information on the edges it is not suited to the current case. Median and Wiener filtering both appear inefficient for the high level of noise in the image: when applied on a small neighborhood the effect is insignificant and if the neighborhood is increase blurring becomes significant and edges cannot be well localized anymore.

5.6 Conclusion

We derive a pre-processing method to reduce noise and enhance some features, namely the colon wall, from our original datasets. We have shown that the most efficient implementation is a scalar anisotropic diffusion technique with Weickert's edge enhancing diffusivity function. This technique has lower restoration strength than the equivalent tensor based technique, but it is preferred because we wish to change the edges as little as possible. Since the edges are the colon wall we are trying to segment, obtaining the most accurate edges is essential in order not to change the shape of the polyps that lie on the colon wall. A main difficulty for the implementation was the big size of the dataset, which is not the most appropriate for an iterative technique. We have derived however an efficient numerical scheme which guarantees stability of the process and allows us to lengthen the step times with minimal loss on accuracy.

Chapter 6

Segmentation of the Colon for Virtual Colonoscopy

6.1 Objectives

The goal of the process is to segment the colon lumen from the patient abdominal dataset in order to construct a complete 3D colon model for visualization. Contemporary approaches should aim at automated segmentation in order to fit into a clinical virtual colonoscopy software.

The process presented in this chapter has the objective to segment the inner boundary of the colon from the images, i.e., the interface between the colon wall and the colon lumen. The colon wall is a soft tissue with a thickness of usually around 2mm, which makes it very difficult to be seen on the current MR datasets, and nearly impossible to segment with good accuracy. A true modeling of the colon would build a model where the colon is represented with its full thickness; however, here we will just create a surface representing the inner interface of the colon, and we will call it the model of the colon. Since the first objective of virtual colonoscopy is to simulate the endoluminal views of an endoscope, obtaining the inner boundary of the colon can be considered as sufficient to test the validity of the process in clinical experiments. We will then see how further features can

be added to a virtual colonoscopy system, either with further processing to the current segmented results or with new segmentation methods. As shown in Section 5.5 the diffusion process tends to segmentation-like results, with piecewise regions in the image. We have seen that it is not possible to push to a higher level in the scale space without degrading the contours and losing valuable information. Thus the segmentation process has to be finished by techniques other than the diffusion. An algorithm for this purpose is proposed in the following section.

6.2 Global Segmentation Algorithm

The core of the adaptive thresholding segmentation algorithm is the local threshold computation which leads to the threshold map, which is then used to obtain the segmentation results. The local threshold computation is based on the properties of the diffusion process, an accurate pre-processed dataset is therefore essential here. A flow chart of the global segmentation algorithm is depicted in Figure 6.1. The first part of the algorithm is the diffusion process (a) which is described in the previous chapter. The rest of the algorithm will use mainly the diffused dataset, as in local threshold computation, to use some properties of the diffusion more efficiently.

Before all, we need to locate the colon in the dataset, what is simple to do for the human eye but is much more difficult to do automatically. The topology of the colon is very convenient since it is basically a simply connected tube with many folds and curves. With a single point inside the colon, we should be able to access all of it without going through the colon wall. In practice collapsed areas and tumors could change significantly this topology so we need more than a single seed point for safety, as provided by the automatic selection seed algorithm (Fig. 6.1(b)) described in Section 6.3.

Numerous routines throughout the segmentation process (such as region growing and morphological operations) will make use of those seeds points showing their importance. For example, some algorithms (Fig. 6.1(d),(i)) might need a

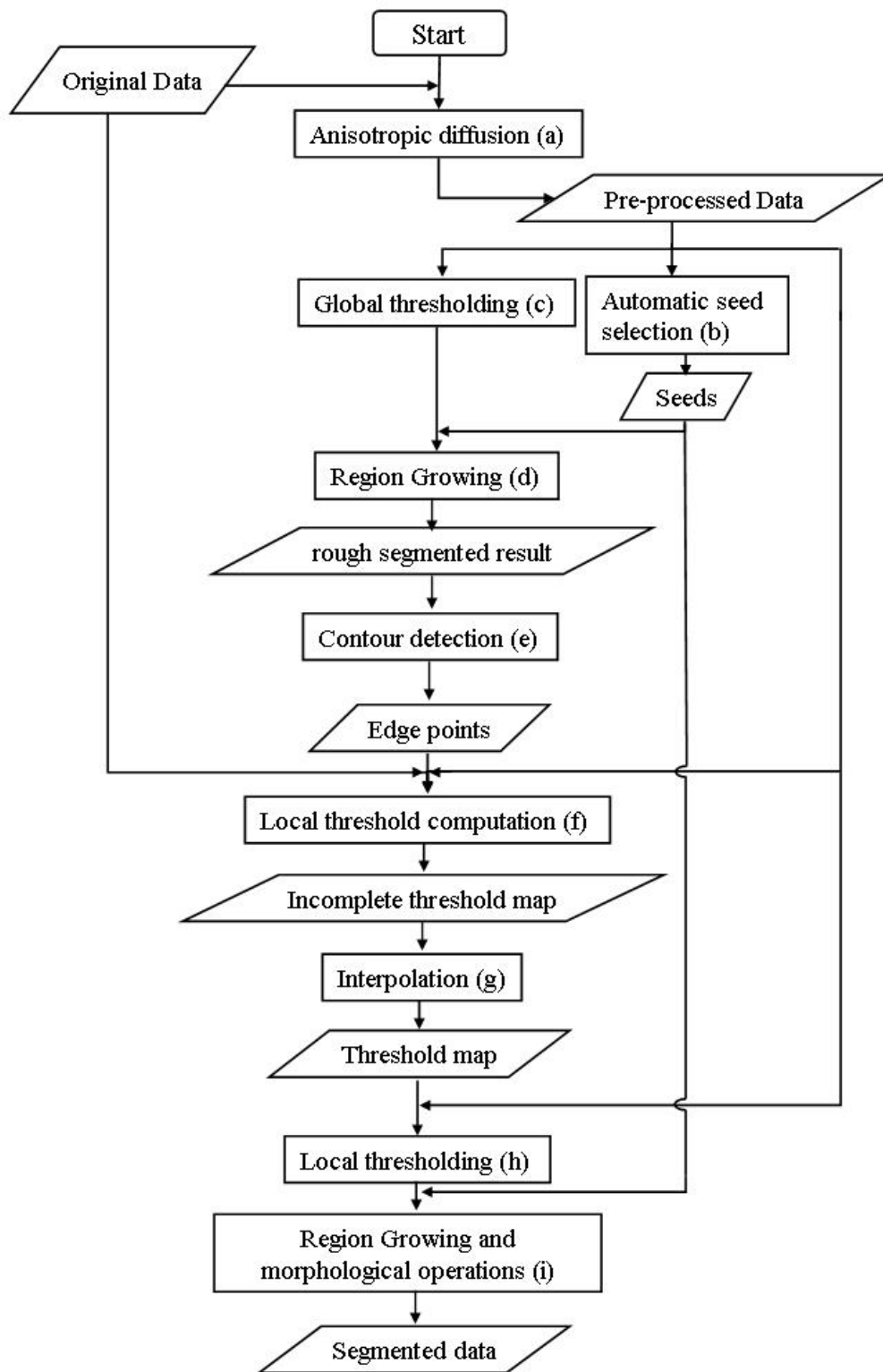


Figure 6.1: Global segmentation algorithm overview

starting point inside the colon and the correctness of the seeds will determine the quality of the final outcome. In most cases it is crucial to set aside some areas that have the same characteristics as the colon and could be misinterpreted as part of it. The processing of those areas would not only increase greatly the computational load but also lead to mis segmented results with unwanted material not part of the colon.

Once the seed points are obtained, we wish to detect automatically a rough approximation of the contours of the colon. Since the dataset resulting from the diffusion process is fairly homogeneous, basic global thresholding (Fig. 6.1(c)) can be applied directly to obtain an approximation of the colon lumen. A region growing operation (Fig. 6.1(d)) starting from the seeds is then also used to constrain the process only to the areas which are connected to the seeds. This first approximation can seem very rough but we are not looking here for a good approximation of the colon wall but just for regions inside the colon lumen.

We detect the contours of the selected areas (Fig. 6.1(e)) in order to select points on those contours which will be used for computation of the local threshold (Fig. 6.1(f)) to establish the threshold map. The number of points used will however be reduced to decrease the computational load and limit redundancy. For each retained point an optimal local threshold is set as defined in Section 6.4 and the thresholding surface is completed using interpolation (Fig. 6.1(g)). The last part of the adaptive thresholding scheme will make use of morphological operations (Fig. 6.1(i)) in addition to the threshold map to segment (Fig. 6.1(h)) the colon from the diffused dataset. The morphological operations used here consist of a closing: dilatation followed by erosion, which is useful to fill in small holes and gaps.

The intermediate results (rough contours, threshold map, etc.) can be seen in Appendix A.

6.3 Automatic Seed Selection

As mentioned previously, seeds inside the colon are essential because they are the foundation on which the rest of the algorithm is constructed. Throughout the algorithm, they set the path so that the result of the segmentation is the colon free of any unwanted material.

The colon is easily recognizable by the human eye in MR images due to these characteristics: it is big, the colon lumen is mainly black, and it has a tube-like shape covered with complicated folds. However these features are not used by algorithms as efficiently as we humans do. Some characteristics make its precise localization especially hard: people come in different sizes, their colon itself can take different shapes and sizes and some parts of the colon can move in the abdomen.

We know from scale space theory that an image is formed of information at different levels of detail, for objects of different sizes and shown at different scales. Since here we are not so much interested in the details of the colon but more in finding an approximate location, the use of a higher scale would be perfectly adequate. To this end we will use the idea behind pyramidal trees, i.e., taking the diffused dataset at a higher scale and lower resolution in order to obtain a new dataset of a much lower size. We will still be able to obtain from the latter the features of interest here: namely, the locations of the colon's lumen.

Using thresholding and morphological operations (dilatation and subtraction) we are able to separate some areas inside the colon from the rest of soft tissues, and map the locations back to the dataset in its original size. It is interesting to note that the use of a dataset of smaller size is here very important because numerous morphological operations are needed and it would be too long and computationally very demanding if done on the full-size image.

6.4 Local Threshold Computation

The local threshold computation process forms the core of the adaptive thresholding algorithm since it will determine the fixed values in the threshold map. The surface will then be interpolated to obtain a full threshold map which can segment the images.

A variety of techniques have been proposed for adaptive thresholding. The minimization of the error between two Gaussian curves chosen to fit the histogram of a subregion is among the most frequent pattern recognition techniques but it is rather costly for numerous local computations on big images. We will obtain inspiration from it to develop a faster scheme.

Yanowitz and Bruckstein [57] made the observation that the optimal local threshold for an edge is to be found in the area of transition of the edge. The difficulty lies however in localizing that area with precision and in finding the average value in the middle of the edge. In most cases we are likely to obtain a value on one side of the edge and not in the middle of it.

The pre-processing diffusion step can however provide us useful information on the contours where we would like the segmentation to operate. We know exactly how the diffusion behaves at the edges since the entire diffusion process has been built around these constraints; i.e., the edge will be sharpened so has to separate the homogenized regions (see Figure 6.2). The two local Gaussian curves that can classically approximate the local edge will therefore tend to two single gray values under the diffusion process. It is then much easier to know all the characteristics of the edge. We know exactly what the edge side values are since the diffusion tends toward it (see Fig. 6.2). Once these values are detected it is easy to get a middle value that would split the edge in two. For more robust detection, the difference between the histogram of the diffused image and the corresponding histogram from the original image is used for analysis instead of just using information from the diffused dataset. This difference is also normalized by the original data to produce a more robust feature. Actually the local neighborhood for which the threshold

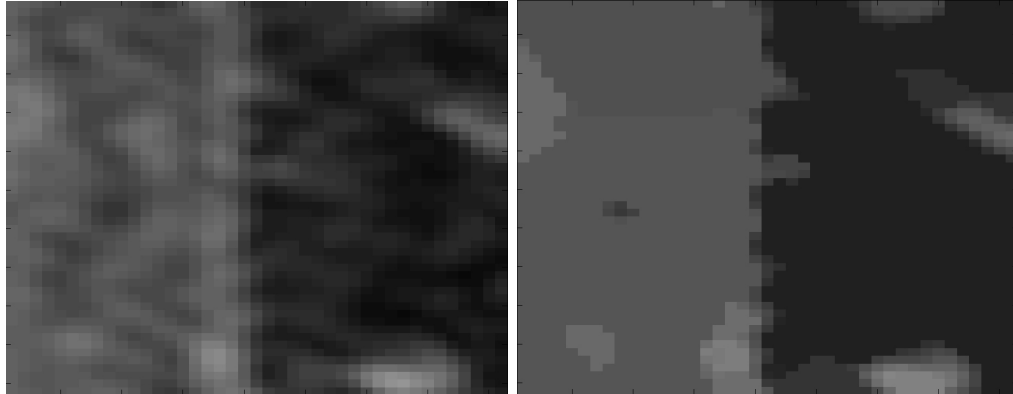
is computed is unlikely to lie exactly on the edge, that is why it is more accurate to work with normalized histograms. Also, in the very noisy cases or those with edges with varying gray levels it gives a stronger descriptor of the diffusion process for more accurate results.

6.5 Results

The segmentation algorithm has been implemented in C++. The total time needed for segmentation on a Pentium IV 3.0 GHz with 1GB of RAM memory running on Windows XP is of 40 minutes. The process has relatively high memory requirements and at least 1GB of RAM is advisable. The reconstructed colon resulting from the segmentation of the dataset used in the previous experiments is shown with the use of 3D rendering techniques in Figure 6.3. An endoscopic view of a polyp lying on the colon wall is also proposed in Figure 6.4. 2D slices of the same data showing the segmented result on top of the original dataset can be consulted in Appendix B.

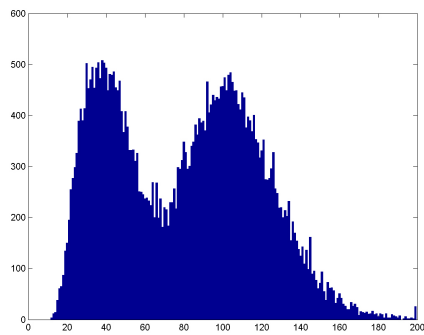
We can see that the colon appears to be fully segmented as one connected surface from the cecum to the rectum. There are no holes in the surface and the folds look natural. The surface also seems to be quite smooth. Though we have seen that the diffusion preprocessing does not provide any smoothing of boundaries; the smooth appearance could be due to the low resolution of the dataset as well as the rendering techniques.

The polyp seen in the endoscopic view has a round shape and should be distinguished easily. After discussion with a radiologist we were told that it is large and lying on the colon wall, which is why it does not protrude from the surface. The view of the radiologist is that the polyp looks realistic. We would like to be sure that the small structures which can be distinguished on the dataset such as polyps are correctly segmented and will be accurately rendered in a virtual colonoscopy system. Clinical requirements show that polyps of 10mm should be detected, while it would be preferable to also obtain a good sensitivity for polyps between 5 to

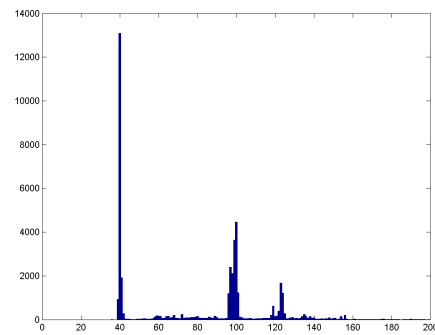


(a) Edge area of an original image

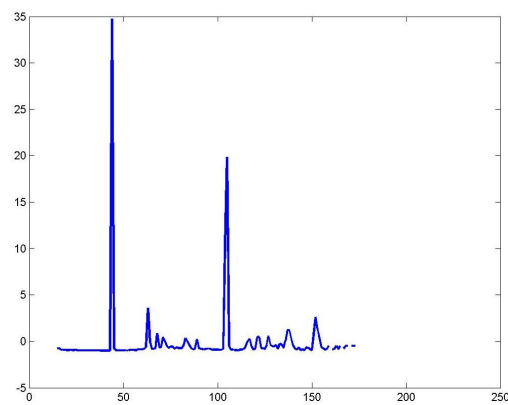
(b) Edge area of the corresponding diffused image



(c) Local histogram of original image



(d) Local histogram of diffused image



(e) Normalized difference of histograms

Figure 6.2: Local features used for adaptive thresholding

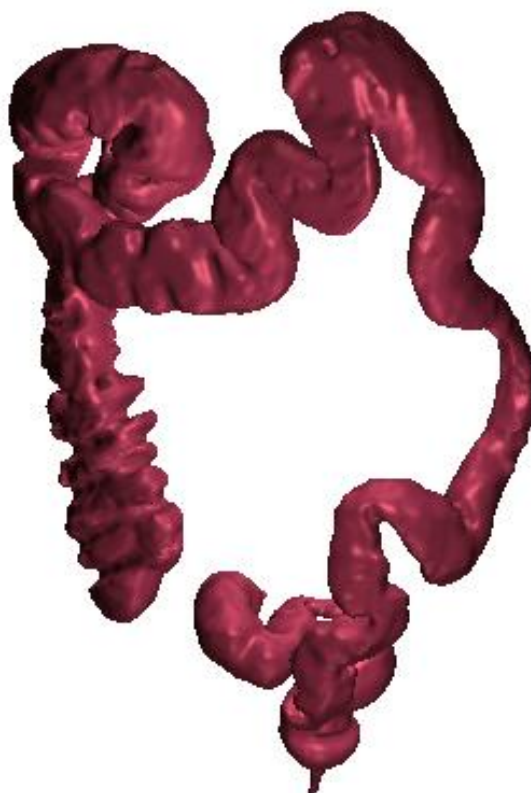


Figure 6.3: Segmented colon

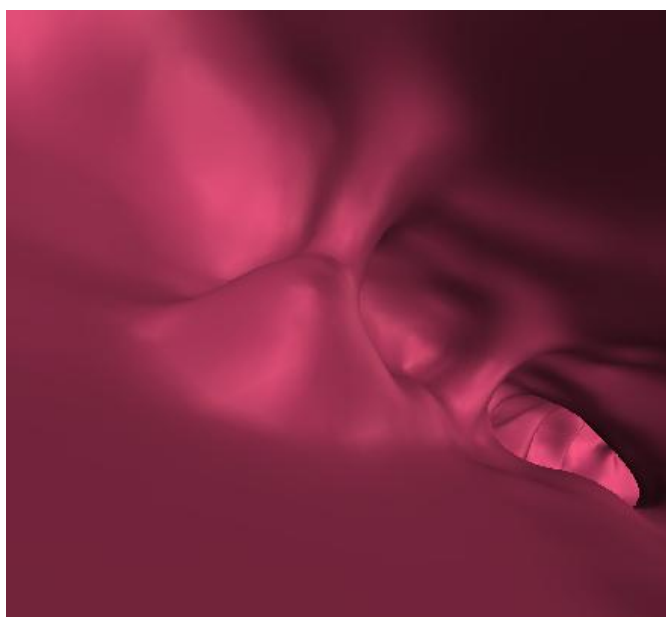


Figure 6.4: Endoscopic view of a polyp

10mm. Since there is no analytical way to know if our implementation can achieve such requirements we would need a radiologist to analyze the segmentation results using his own knowledge to validate the process.

6.6 Discussion

6.6.1 Consequences of diffusion on the segmentation results

The diffusion process plays a fundamental role in the segmentation toward the construction of a 3D model. The MR dataset has originally an inconvenient inhomogeneity artifact which is prejudicial to the segmentation. Combined with the wide range of intensity values that the colon wall can take, it prevents the use of a global contrast enhancement method that would not operate optimally on the full dataset, possibly even deteriorating the information in the areas that are badly affected by the inhomogeneity. The latter is removed partially with the diffusion process and we could think that a global thresholding scheme would be sufficient to complete of the segmentation; however the size of the dataset and the many differences in intensities of the colon wall itself make it inappropriate.

When having to set a global threshold for the full dataset, the inhomogeneity forces it to be very low. In some areas the soft tissues have gray values very proximate to other noisy areas inside the colon lumen. If we set a threshold value that would be near optimality for the majority of edges, some soft tissues could be badly segmented and the segmentation could leak outside the colon. On the contrary, if the threshold is set very low, we are likely to missegment some area and perform an non optimal segmentation for the majority of edges. The segmentation cannot therefore be completed with a simple thresholding scheme after diffusion. As detailed in Section 6.4, the properties of the diffusion provide us a adaptive thresholding framework to work on.

The strength of the preprocessing step is therefore double; not only does it

reduce the noise level considerably, but the adaptive thresholding scheme also relies entirely on its edge properties.

It is also important to note that the edge enhancement property of anisotropic diffusion acts naturally toward removing the partial volume effects. With a straighter edge the uncertainties usually brought into the segmentation process by PVE are considerably reduced without the need of additional heuristics.

6.6.2 Reliability of the segmentation process

As for all automated processes, reliability concerns of the entire segmentation process have to be investigated. First, we note that the segmentation relies entirely on the preprocessing diffusion step. We therefore have to make sure that the entire diffusion process is performed the most accurately. The robustness of the diffusion algorithm is an important point, with the main concern being the very thin structures in the image that must not be smoothed. When the colon is badly distended it can happen that different part of the colon are in contact. Taking into account the thickness of the colon wall which is around 2mm, it creates structures that may be smaller than smallest polyps we are trying to detect and it could lead to these structures being smoothed by the diffusion process. Even if a radiologist would have no difficulty in detecting it as it does not look natural and cannot correspond to any pathology of the colon, it is a major drawback because it will jeopardize the outcome of the algorithm.

We have seen how the region growing algorithms rely on the topology of the colon to separate the colon lumen from unwanted materials. If a boundary is smoothed the topology changes and the region growing process will leak outside the colon. A stopping criteria would have to be implemented in order to contain the leak that can compromise the full segmentation process. When a leak occurs, apart from mis-segmenting the colon, it creates new edges outside the colon; if the leak is important it can lengthen considerably the duration of the segmentation and possibly lead the process to run out of memory.

It can be very difficult to perform the segmentation of the colon exclusively of unwanted material. When seeds are automatically selected, it can happen that the small intestine is mistakenly considered as part of the colon. The results will show part of the small intestine, which is not a major drawback however because it can be easily recognized by the radiologists. Manual seed selection could solve the problem in that case.

6.7 Use of Segmentation Results in Virtual Colonoscopy

6.7.1 Conventional use

Once the colon is segmented in the 3D dataset, the visualization and analysis part of virtual colonoscopy come into play. These are globally indifferent from any techniques used in any other virtual colonoscopy software. No matter which is the imaging protocol, we wish to reconstruct a colon model to aim at the same virtual navigation inside the colon.

Rendering techniques have to be used for visualization of 3D data. Surface rendering techniques using the segmented results and based on the marching cubes algorithm or adaptive skeleton climbing are among the most commonly used, and the latter is the one being used in the software developed internally [58].

Different views can be used for examination, but endoscopic views (Figure 6.5) are the most liked by the physicians since they simulate a real endoscopy which they are used to. A user friendly environment (Figure 6.6) must also be provided for examination purposes providing real time rendering and interactivity which are essential requirements. Through a user-friendly interface, the radiologist should be able to navigate freely to search for polyps within the colon. To this end, automatically extracted flight path based on the medial axis computed on the segmented colon is necessary to provide automatic navigation for ease of visualization.



Figure 6.5: Endoscopic view of the segmented colon

Discussion with physicians show that they rely importantly on the cross sectional views to spot areas at risk. The software should therefore incorporate such views on which the segmented information can be superposed as in Figure 6.6. This is important because the radiologist should always have the possibility to check the results of the automatic segmentation process when in doubts.

The use of the segmented results is however not restricted to visualization procedures and medial axis computation, and further information can be extracted from the segmented data to be at the clinician's disposition during the examination. Polyp detection algorithms are for instance an active area of research today. The idea is to go through the segmented colon to automatically detect polyps or least list potential polyps candidates. The polyps found can then be indicated to the physician on the virtual colonoscopy software for him to go directly and focus on the areas at risk during examination, saving him valuable time required otherwise to spot polyps in the data. It follows that an accurate polyp detection scheme

would help achieving very high sensitivity rates, making virtual colonoscopy a more reliable procedure.

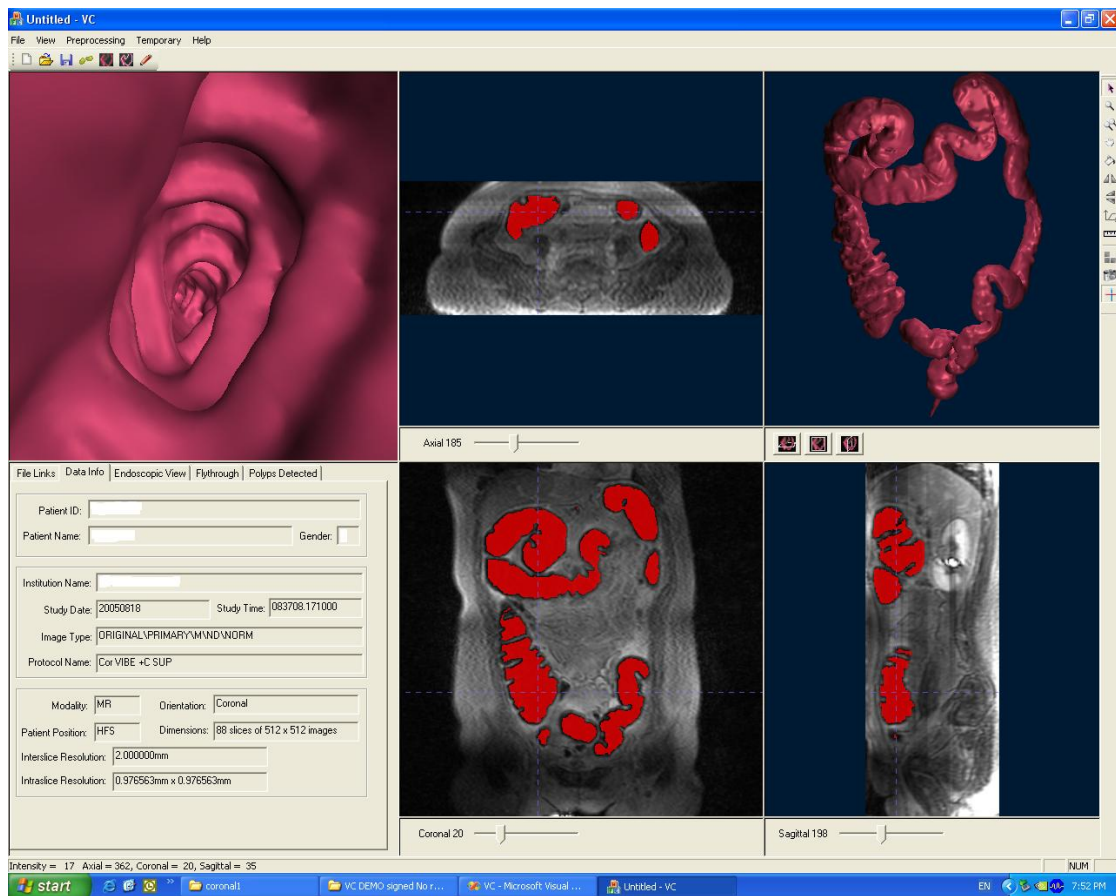


Figure 6.6: Virtual colonoscopy software

6.7.2 Future Work

MR screening techniques opens new horizons for virtual colonoscopy. When analyzing MR abdominal images, the physician looks at the shape of the colon wall to detect polyps and tumors, and usually also uses the change in intensities to help his judgment. The unrivaled imaging of soft tissues offered by MRI, combined with the further injection of contrast agent, opens the path to distinguishing the colon wall entirely and not just by its inner boundary delimiting the colon lumen, as it is done for CT based techniques which offer very low contrast between soft tissues. The tumors and polyps show in almost all cases an increase in thickness of the colon wall compared to a healthy colon wall, giving additional information for

examination. The colon wall intensity can also give meaningful knowledge about the visualized areas, since polyps, tumors or unwanted materials (remaining fluids, faeces, etc.) can sometimes appear with different intensities indicating a region to be analyzed with care to the radiologist.

Those observations could be expanded into new features for a virtual colonoscopy software providing an enhanced examination environment.

First the intensity of the inner surface of the colon wall could be mapped onto the reconstructed model. Instead of showing endoscopic views of a single colored model we would experience something closer to real colonoscopy. Getting the local intensity of the soft tissues is a fairly straight forward operation considering the operations done previously. When computing the local threshold we just need to keep the value of the side of the edge (corresponding to the colon wall) and link it to the corresponding location. Similarly to how the threshold surface is completed, we can get a intensity surface that we will map onto the reconstructed colon. This feature is based on information extracted from the diffused dataset rather than the original one, we would therefore be viewing an average local intensity instead of the precise colon wall intensity. The impossibility to distinguish the colon wall with precision in the original data due to high noise level and low resolution is at the origin of this drawback; if the colon wall is hardly or not recognizable it is likely to be merge with some adjacent tissues in the diffused dataset. This is not a major concern however since the use of the technique is not to show with exactitude the colon wall's intensity but more to highlight the regions at risk; and if a region had a change in intensity it would be shown by this technique.

Another feature to which physicians look forward to with great expectations is getting data about the colon wall thickness. It is known that areas with polyps and tumors correspond to an increase in the colon wall's thickness. If we could extract that information from the datasets and color code it into the model we would be able to provide an endoscopic with an additional detection feature coded into another dimension in the model. This would create true value to MR virtual

colonoscopy since it would give information that conventional colonoscopy and even CT colonography cannot access. Regions at risk would be much more easily identifiable, giving globally a more powerful visualization technique, increasing the sensitivity of the process while reducing the examination time for the physicians. The main problem with this feature is that the current technology does not enable us to measure the colon wall's thickness. While it can be identified in very few cases by the human eye, major improvements will still be needed to implement that feature automatically in a virtual colonoscopy software.

Lastly, there is also major on going research on automatic polyp detection. Integrating all the above mentioned information on the regions at risk of the colon into an automatic software for polyp detection has to be considered the ultimate goal of VC systems. The work of physicians would then be greatly enhanced by reducing considerably the time needed to analyze each dataset. He could focus directly on regions at risk, with all the information at his disposal for diagnosis thanks to advanced 3D rendering techniques. This kind of human machine cooperation will drive the development of wide spread MR based VC systems.

Chapter 7

Conclusion

We have presented a method based on anisotropic diffusion techniques to segment the colon from abdominal MR volumetric datasets in view of their use for virtual colonoscopy. This method can be divided into two major phases: a pre-processing step which enhances the important features of the colon, followed by a segmentation step which extracts the inner boundary of the colon in view of constructing a 3D model of the colon.

The strength of the diffusion technique is that it is used in both phases: While the anisotropic diffusion process forms the first phase by itself, the second phase is based on its properties to yield a segmentation scheme.

The difficulty of using MR images for virtual colonoscopy comes from the adverse characteristics of the images which prevents easy segmentation of the colon. We have shown how the scale space created by the diffusion process can provide a framework which can enhance the features needed for segmentation by reducing the important noise level and enhancing the contours of the colon. However much care is needed to develop a scale space suitable under the numerous constraints: we have seen for example how the restoration properties of the tensor scheme loses information on the contours or how the features are best at a certain level in the scale space. We have also managed to get a numerical implementation of the process which offers stability and that is adapted to the big size of our datasets.

The tenuous work needed to yield a good diffusion is leveraged when deriving the segmentation process. An adaptive thresholding scheme is developed based on the enhancement properties of the diffusion process making possible the segmentation of the inner boundary of the colon. The validation of the process is a difficult task since it would require a radiologist to analyze the quality of the outcome based on his own knowledge. It is nonetheless imperative to assess the reliability of the process to be sure that polyps bigger than 10 mm and possibly than 5mm can be detected.

Some improvements could be proposed to develop a more efficient scheme. For images of such characteristics the pre processing step seems essential to perform the segmentation. Nonetheless, the segmentation proposed is only intensity based, more advanced schemes which would take spatial information into account should help getting more precise results. Letting aside the technical constraints the use of Gradient Vector Flow deformable models could for example be well suited to the problem, since they use spatial information as well as the diffusion process to steer the deformable model. Active contours are certainly one of the key areas to be investigated to be able to measure the performance of the current segmentation process.

The outcome of the segmentation process is also restricted for now to the inner boundary of the colon. With such information, a virtual colonoscopy system can be implemented with the conventional endoscopic views, automatic flight path and possibly even automatic polyp detection features. However all those features can already be found in commercial CT virtual colonoscopy systems. The true value of an MR based system would lie not only in its radiation free acquisition protocol, but most importantly in the additional features it would bring, predominantly the thickness of the colon wall. However the quality of the datasets is such that in most cases today we cannot distinguish the colon wall except from its inner boundary which does not give the opportunity for advanced features. The limitations of the acquisition technique, being mainly the length of the acquisition time and the

resolution of the datasets are key issues and they are quite unlikely to change in the near future, preventing the wide spread of MR based VC systems. The rationale of an MR virtual colonoscopy system is still dependent on major technological improvements of data acquisition.

Appendix A

Intermediate Results of the Segmentation Algorithm

The intermediate results of the segmentation process are presented for one slice of a dataset.



Figure A.1: Seed points resulting from automatic seed selection

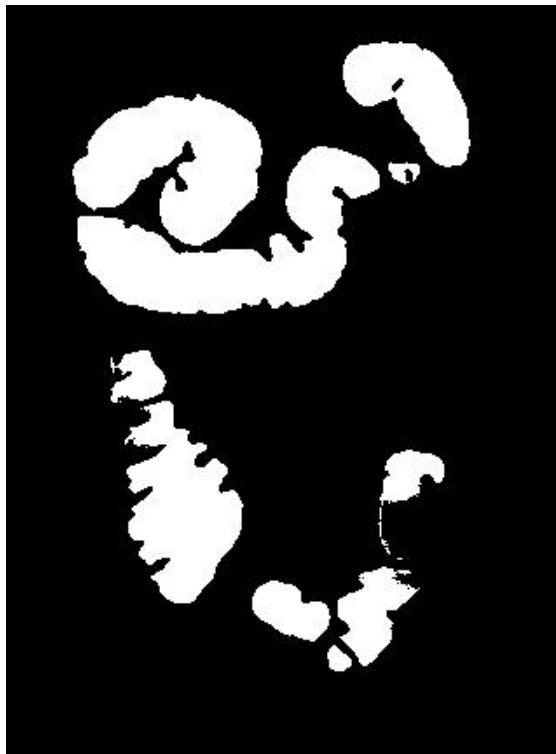


Figure A.2: Rough segmented colon after global segmentation and region growing



Figure A.3: Incomplete threshold map after computation of thresholds at the edge points

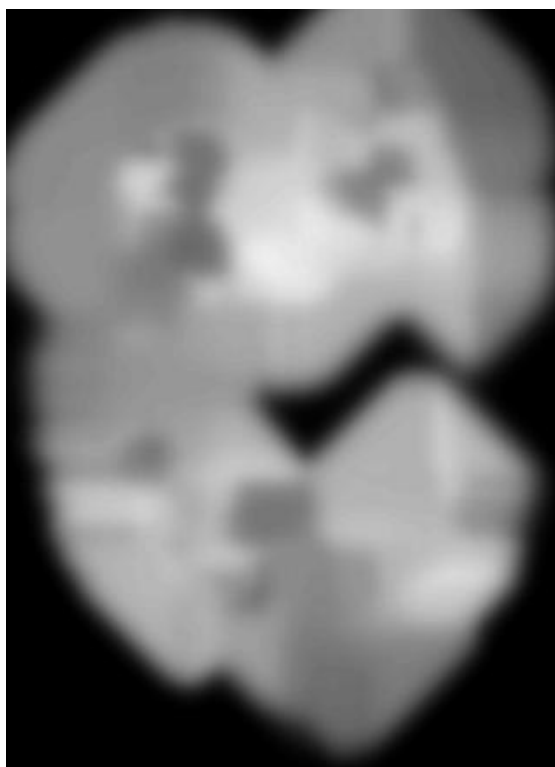


Figure A.4: Complete threshold map after interpolation

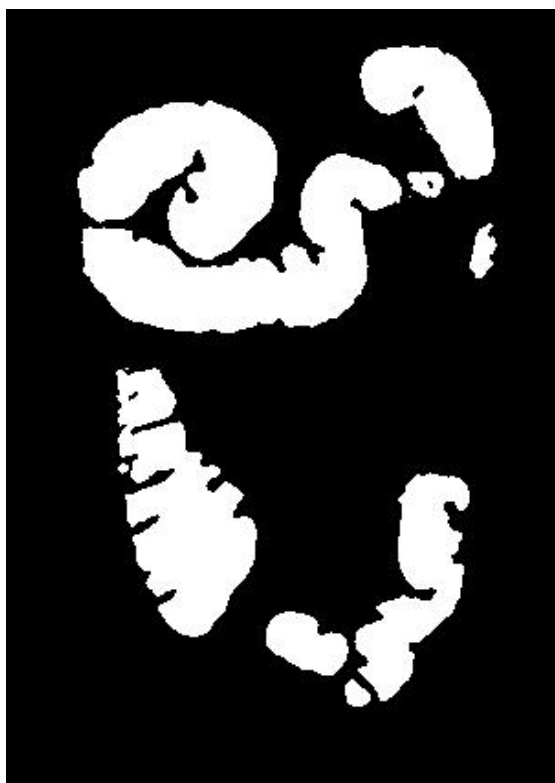


Figure A.5: Final segmented result after adaptive thresholding and region growing

Appendix B

Segmentation Results

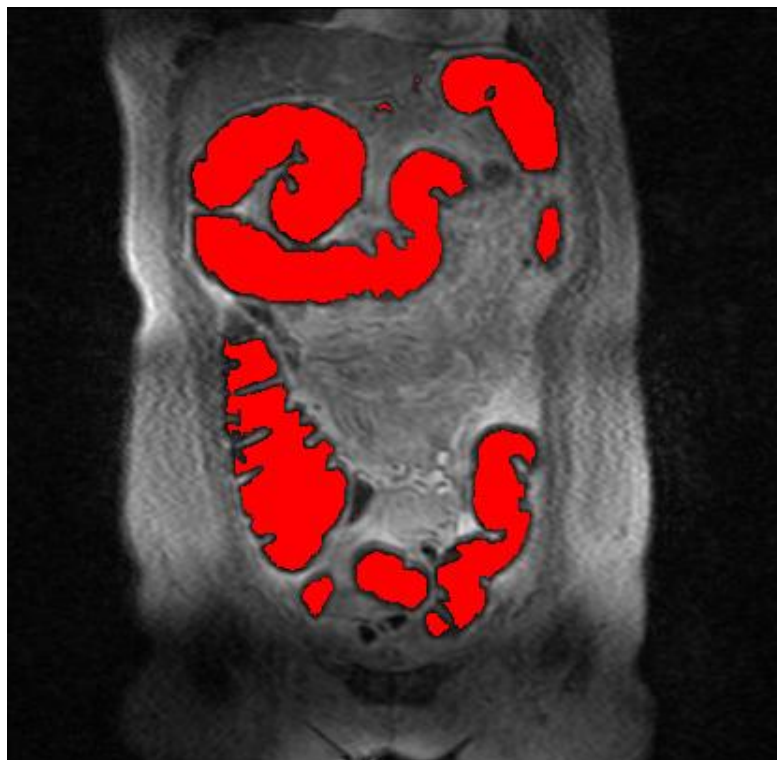


Figure B.1: Segmented result of slice 19 of dataset MRC712

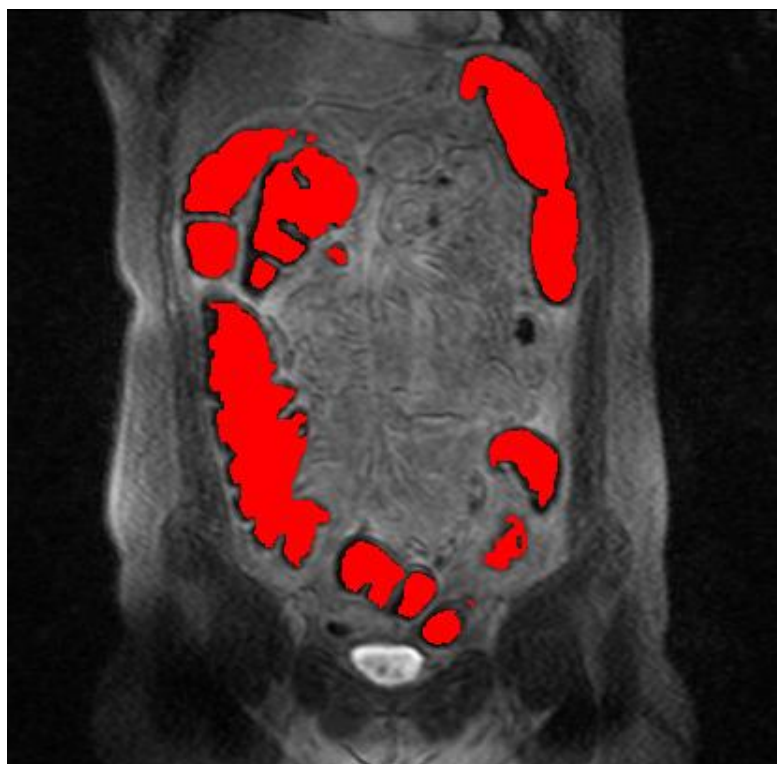


Figure B.2: Segmented result of slice 27 of dataset MRC712

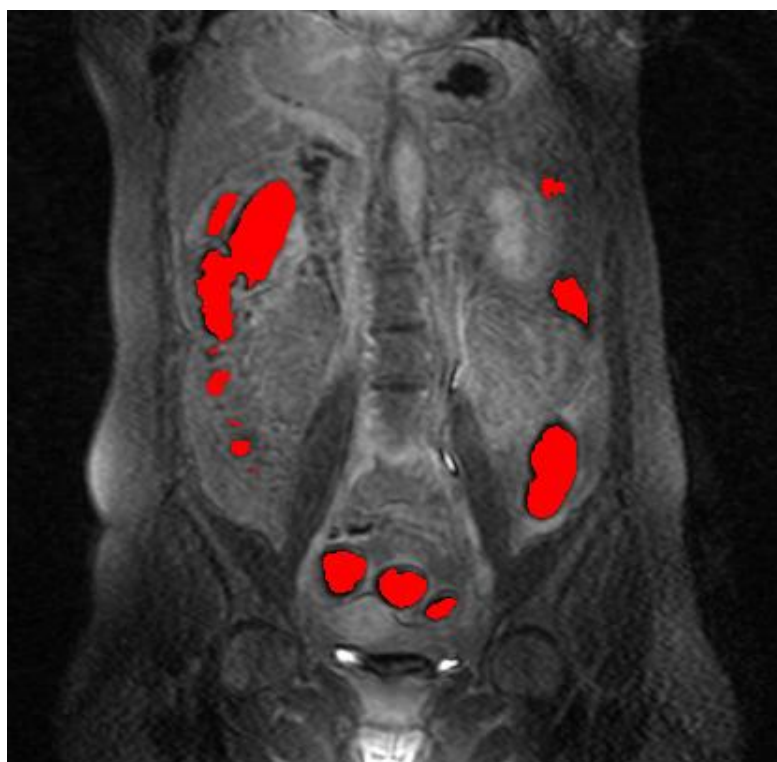


Figure B.3: Segmented result of slice 41 of dataset MRC712



Figure B.4: Segmented result of slice 60 of dataset MRC712

Bibliography

- [1] E. Ward and V. Cokkinides, “Colorectal cancer facts and figures,” Atlanta, US, 2005.
- [2] S. Landis, T. Murry, S. Bodden, and et al, “Cancer statistics, 1998,” *Cancer Journal for Clinicians*, vol. 48, pp. 6–29, 1998.
- [3] L. Rosen, “Screening and surveillance for colorectal cancer,” Arlington Heights, IL, US, 2002.
- [4] C. Becker, M. Schatzl, H. Feist, and et al, “Radiation exposure during ct examination of thorax and abdomen. comparison of sequential, psiral and electron beam computed tomography,” *Radiologe*, vol. 38, pp. 726–729, 1998.
- [5] D. Brenner and M. Georgsson, “Mass screening with ct colonography: Should the radiation exposure be of concern?” *Gastroenterology*, vol. 129, pp. 328–337, 2005.
- [6] T. Lauenstein, “Mr colonography: current status,” *European Radiology*, vol. 16, pp. 1519–1526, July 2006.
- [7] W. Lubold and et al., “Colonic masses: detection with mr colonogrphahy,” *Radiology*, vol. 216, pp. 383–388, 2000.
- [8] G. Pappalardo and et al., “Magnetic resonance colonography versus conventional colonoscopy for the detection of colonic endoluminal lesions,” *Gastroenterology*, vol. 119, pp. 300–304, 2000.

- [9] D. Chen, T. Button, H. Li, W. Huang, and Z. Liang, "Mr imaging and segmentation of the colon wall for virtual colonoscopy," *Proc. International Society of Magnetic Resonance in Medicine*, vol. 3, p. 2203, 1999.
- [10] N. Rofsky, V. Lee, G. Laub, M. Pollack, G. Krinsky, D. Thomasson, M. Ambrosino, and J. Weinreb, "Abdominal mr imaging with a volumetric interpolated breath-hold examination," *Radiology*, vol. 212, pp. 876–884, 1999.
- [11] W. Ajaj, T. Lauenstein, G. Pelster, S. Goehde, J. Debatin, and S. Ruehm, "Mr colonography: How does air compare to water for colonic distention?" *Journal of Magnetic Resonance Imaging*, vol. 19, pp. 214–221, 2004.
- [12] T. Lauenstein, C. Herborm, F. Vogt, S. Goehde, J. Debatin, and S. Ruehm, "Dark lumen mr colonography: initial experience," *Rofo Fortschr Geb Roentgenstr*, vol. 173, pp. 785–789, 2001.
- [13] J. Montagnat, M. Sermesant, H. Delingette, G. Malandain, and N. Ayache, "Anisotropic filtering for model-based segmentation of 4D cylindrical echocardiographic images," *Pattern Recognition Letters - Special Issue on Ultrasonic Image Processing and Analysis*, vol. 24, no. 4-5, pp. 815–828, February 2003.
- [14] U. Clarenz, U. Diewald, and M. Rumpf, "Anisotropic geometric diffusion in surface processing," in *Proceedings of Visualization 2000*, T. Ertl, B. Hamann, and A. Varshney, Eds., 2000, pp. 397–405.
- [15] G. Gerig, R. Kikinis, O. Kbler, and F. Jolesz, "Nonlinear anisotropic filtering of mri data," *IEEE Transactions on Medical Imaging*, vol. 11, no. 2, pp. 221–232, June 1992.
- [16] K. Krissian, "Diffusion anisotrope d'images cérébrales 3D et segmentation matière blanche / matière grise," Rapport de DEA, université de Paris IX, septembre 1996.

- [17] F. Catte, P. Lions, J. Morel, and T. Coll, "Image selective smoothing and edge detection by nonlinear diffusion," *SIAM Journal of Numerical Analysis*, vol. 29, pp. 182–193, 1992.
- [18] C. Xu and J. Prince, "Snakes, shapes, and gradient vector flow," pp. 359–369, 1998.
- [19] S. Manay and A. Yezzi, "Anti-geometric diffusion for adaptative thresholding and fast segmentation," *IEEE Transactions on Image processing*, vol. 12, pp. 1310–1323, Nov 2003.
- [20] M. Clark, L. Hall, D. Goldgof, L. Clarke, R. Velthuisen, and M. Silbiger, "Mri segmentation using fuzzy clustering techniques," *IEEE Engineering in Medicine and Biology Magazine*, vol. 13, pp. 730–742, 1994.
- [21] R. Herndon, J. Lancaster, J. Giedd, and P. Fox, "Quantification of white matter and gray matter volumes from three-dimensional magnetic resonance volume studies using fuzzy classifiers," *Journal of Magnetic Resonance Imaging*, vol. 8, pp. 1097–1105, 1998.
- [22] Z. Liang, J. MacFall, and D. Harrington, "Parameter estimation and tissue segmentation from multi spectral mr images," *IEEE Transactions on Medical Imaging*, vol. 13, pp. 441–449, 1994.
- [23] K. Held, E. Kops, B. Krause, W. Wells, R. Kikinis, and H.-W. Muller-Gartner, "Markov random field segmentation of brain mr images," *IEEE Transactions on Medical Imaging*, vol. 16, pp. 878–886, December 1997.
- [24] L. Li, D. Chen, K. K. S. Lakare, I. Bitter, A. Kaufman, M. R. Wax, P. M. Djuric, and Z. Liang, "An image segmentation approach to extract colon lumen through colonic material tagging and hidden markov random field model for virtual colonoscopy," in *SPIE 2002 Symposium on Medical Imaging*, San Diego, CA, February 2002.

- [25] M. Sermesant, “Modèle électromécanique du coeur pour l’analyse d’image et la simulation,” Thèse de sciences, université de Nice Sophia-Antipolis, May 2003.
- [26] M. Rousson, N. Paragios, and R. Deriche, “Implicit active shape models for 3d segmentation in mr imaging,” in *MICCAI*, Rennes - Saint Malo France, September 2004.
- [27] C. Xu and J. L. Prince, “Snakes, shapes, and gradient vector flow,” *IEEE Transactions on Image Processing*, vol. 7, no. 3, pp. 359–369, March 1998.
- [28] T. McInerney and D. Terzopoulos, “Deformable models in medical image analysis: a survey.” *Medical Image Analysis*, vol. 1, no. 2, pp. 91–108, June 1996.
- [29] J. Montagnat, H. Delingette, N. Scapel, and N. Ayache, “Representation, shape, topology and evolution of deformable surfaces. application to 3d medical image segmentation.” INRIA, technical report RR-3954, May 2000.
- [30] G. Gazelle, P. McMahon, and F. Scholz, “Screening for colorectal cancer,” *Radiology*, vol. 215, pp. 327–335, 2000.
- [31] W. Press, B. Flannery, S. Teukolsky, and W. Vetterling, *Numerical Recipes in C++: The Art of Scientific Computing*. Cambridge University Press, 1993, ch. 3.
- [32] J. Weickert, “Anisotropic diffusion in image processing,” Ph.D. dissertation, Dept. of Mathematics, University of Kaiserslautern, Germany, 1996.
- [33] P. Perona and J. Malik, “Scale-space and edge detection using anisotropic diffusion,” *Pattern Analysis and Machine Intelligence, IEEE Transactions on*, vol. 12, no. 7, pp. 629–639, 1990.

- [34] K. Krissian, “Traitement multi-échelle : Applications à l’imagerie médicale et à la détection tridimensionnelle de vaisseaux,” Thèse de sciences, université de Nice Sophia-Antipolis, Janvier 2000.
- [35] A. Witkin, “Scale-space filtering,” in *8th Int. Joint Conference on Artificial Intelligence*, vol. 2, August 1983, pp. 1019–1022.
- [36] J. Koenderink, “The structures of images,” *Biological Cybernetics*, vol. 50, pp. 360–370, 1984.
- [37] A. Yuille and T. Poggio, “Scaling theorems for zero-crossings,” *IEEE Transactions on Pattern Analysis and Machine Intelligence*, vol. 8, pp. 15–25, 1986.
- [38] T. Lindeberg, *Scale-space theory in computer vision*. Kluwer, Netherlands, 1994.
- [39] L. Florack, “The syntactical structure of scalar images,” Dept. Med. Phys., University of Utrecht, 1993.
- [40] P. J. Burt, “Fast filter transforms for image processing,” *Computer Graphics and Image Processing*, vol. 16, pp. 20–51, 1981.
- [41] R. Finkel and J. Bentley, “Quad trees: A data structure for retrieval on composite keys,” *Acta Informatica*, vol. 4, pp. 1–9, 1974.
- [42] A. Witkin, “Scale space filtering: a new approach to multi-scale description,” *Proc. IEEE International Conference on Acoustics, Speech, Signal Processing*, vol. 9, pp. 150–153, 1984.
- [43] J. Weickert, S. Ishikawa, and A. Imiya, “Linear scale-space has first been proposed in japan,” *Journal of Mathematical Imaging and Vision*, vol. 10, no. 3, pp. 237–252, 1999.
- [44] J. Weickert, *Anisotropic Diffusion in Image Processing*. Teubner, 1998.

- [45] T. Lindeberg, "Scale-space theory: A basic tool for analyzing structures at different scales," *Journal of Applied Statistics*, vol. 21(2), pp. 224–270, 1994, (Supplement on Advances in Applied Statistics: Statistics and Images: 2).
- [46] L. Alvarez, F. Guichard, P. Lions, and J. Morel, "Axioms and fundamental equations of image processing," *Archives of Rational and Mechanical Analysis*, vol. 123, pp. 200–257, 1993.
- [47] R. Malladi, J. Sethian, and B. Vemuri, "Shape modeling with front propagation: A level set approach," *IEEE Transactions on Pattern Analysis and Machine Intelligence*, vol. 17, no. 2, pp. 158–175, 1995.
- [48] L. Alvarez and J. Morel, "A morphological approach to multiscale analysis: From principles to equations," *Kluwer Academic Publishers*, vol. 6.5.2, pp. 229–254, 1994.
- [49] K. Nordstrom, "Biased anisotropic diffusion: a unified regularization and diffusion approach to edge detection," *Image Vision Computing*, vol. 8, no. 4, pp. 318–327, 1990.
- [50] G. Arfken, *Mathematical Methods for Physicists*, 3rd ed. Orlando, FL: Academic Press, 1985.
- [51] P. Charbonnier, L. Blanc-Feraud, G. Aubert, and M. Barlaud, "Deterministic edge-preserving regularization in computed imaging," *IEEE Transaction on Image Processing*, vol. 6, pp. 298–311, 1997.
- [52] M. J. Black, G. Sapiro, D. H. Marimont, and D. Heeger, "Robust anisotropic diffusion," *IEEE Transactions on Image Processing*, vol. 7, no. 3, pp. 421–432, March 1998.
- [53] S. Kichenassamy, "The perona-malik paradox," *SIAM Journal of Applied Mathematics*, vol. 57, no. 5, pp. 1328–1342, 1997.

-
- [54] J. Weickert and B. Benhamouda, “A semidiscrete nonlinear scale-space theory and its relation to the perona–malik paradox,” pp. 1–10, 1997.
- [55] J. Weickert, B. Romeny, and M. Viergever, “Efficient and reliable schemes for nonlinear diffusion filtering,” *IEEE Transactions on Image Processing*, vol. 7, no. 3, pp. 398–410, March 1998.
- [56] P. Mrázek and M. Navara, “Consistent positive directional splitting of anisotropic diffusion,” in *Computer Vision Winter Workshop*, B. Likar, Ed. Slovenian Pattern Recognition Society, Feb 2001, pp. 37–48.
- [57] S. D. Yanowitz and A. M. Bruckstein, “A new method for image segmentation,” *Computer Vision, Graphics, and Image Processing*, vol. 46, no. 1, pp. 82–95, 1989.
- [58] Y. E. Thiam, “Virtual colonoscopy software,” Bachelor of Engineering, National University of Singapore, May 2004.